Received 19 January 2025; revised 24 February 2025; accepted 13 March 2025. Date of publication 24 March 2025; date of current version 7 April 2025.

Digital Object Identifier 10.1109/OJCOMS.2025.3554077

Extending the LoRa Direct-to-Satellite Limits: Doppler Shift Pre-Compensation

MUHAMMAD ASAD ULLAH [1] (Member, IEEE), RICHARD DEMO SOUZA [2] (Senior Member, IEEE), GIANNI PASOLINI [3] (Member, IEEE), JEAN MICHEL DE SOUZA SANT'ANA [4] (Member, IEEE), MARKO HÖYHTYÄ [5] (Senior Member, IEEE), KONSTANTIN MIKHAYLOV [4] (Senior Member, IEEE), HIRLEY ALVES [4] (Member, IEEE), ENRICO PAOLINI [3] (Senior Member, IEEE), AND AKRAM AL-HOURANI [6] (Senior Member, IEEE)

[1]VTT Technical Research Centre of Finland Ltd., 02044 Espoo, Finland
[2]Electrical and Electronics Engineering Department, Federal University of Santa Catarina, Florianopolis 88040-900, Brazil
[3]CNIT/WiLab, Department of Electrical, Electronic, and Information Engineering, University of Bologna, 40136 Bologna, Italy
[4]Centre for Wireless Communications, University of Oulu, 90014 Oulu, Finland
[5]Military Technology Department, Finnish National Defence University, 00860 Helsinki, Finland
[6]Department of Electrical and Electronic Engineering, RMIT University, Melbourne, VIC 3000, Australia

CORRESPONDING AUTHOR: M. A. ULLAH (e-mail: Asad.Ullah@vtt.fi)

This work was supported in part by the Business Finland through the 6G-SatMTC and Drolo II Projects; in part by the European Union through the Interreg Aurora Project ENSURE-6G under Grant 20361812; in part by 6G Flagship funded by the Research Council of Finland under Grant 369116; in part by RNP/MCTI Brasil 6G Project under Grant 01245.020548/2021-07; in part by Print CAPES-UFSC "Automation 4.0"; and in part by CAPES/STIC-AMSUD.

ABSTRACT Earlier studies and field tests have extensively investigated Long Range (LoRa) direct-to-satellite (DtS) communications, confirming the feasibility of integration with Low Earth Orbit (LEO) satellites. These works identify the Doppler effect as one of the primary challenges. Therefore, there is a need for a robust solution to mitigate the impact of this phenomenon in order to improve the performance of LoRa DtS communications in a LEO scenario. This paper addresses this shortcoming by developing a solution to pre-compensate the Doppler shift. Specifically, we propose a method that allows end devices to estimate and pre-compensate the Doppler shift before initiating an uplink transmission. This framework, which requires satellites to broadcast Doppler Beacons, ensures compatibility with existing LoRaWAN end devices without requiring any hardware modifications. We leverage data from real-world LoRa satellites' empirical telemetry to validate our proposed method. We analytically study packet losses due to Doppler shift across different carrier frequencies, specifically 401.5 MHz, 868 MHz, and 2 GHz. Our analysis also considers different satellite orbital heights, specifically 200 km and 518 km, as well as channel bandwidths of 31.25 kHz, 62.5 kHz, and 125 kHz. Our results demonstrate that the proposed solution effectively pre-compensates for the Doppler shift and mitigates the packet losses, extending the passing satellites' effective visibility window duration. We examine the maximum Doppler shift in the communication channel and the calculate required Doppler Beacon bandwidth for different orbital altitudes, minimum elevation angles, and carrier frequencies. This study also investigates how the proposed framework affects the battery lifetime of the end device, showing a marginal decrease of 2.5% compared to traditional LoRaWAN operation.

INDEX TERMS Direct-to-satellite, Doppler estimation, doppler compensation, LEO, LoRaWAN.

I. INTRODUCTION

LORA is a modulation scheme used by Long Range Wide Area Network (LoRaWAN), one of the most popular and widely adopted low-power wide-area network (LPWAN) technologies. Known for its low power consumption and long-range communication capabilities [1], [2], [3], [4], [5], [6], [7], [8], LoRaWAN has become the de facto standard for terrestrial Internet-of-Things (IoT) applications. However, the characteristics of LoRa modulation, combined with its use in unlicensed bands, make LoRa a promising and

cost-effective choice also in the expanding landscape of direct-to-satellite (DtS) IoT technologies [3], [9], [10]. In the new space era, LoRa DtS communications bridge the digital divide and hold the potential to offer global coverage for IoT end devices in remote areas. In fact, as of January 2025, there are hundreds of active LEO satellites featuring LoRa modulation, including Lacuna Space, Norby, TIANQI, and GaoFen, to name a few [11], [12], [13], [14]. These satellites transmit periodically, and as of the time of writing this article, thousands of end devices have received over twenty-two million LoRa packets from space [15].

Although experimentation is at an advanced stage, multiple critical issues remain that limit the full exploitation of this technology in the realm of satellite communications, particularly massive interference [16] and the strong Doppler shift effect. Existing studies mainly focus on link budget [17] and network scalability aspects [18], [19], [20]. In contrast, only a few have investigated the impact of the Doppler effect on LoRa DtS performance and identified the boundaries for successful operation in the LEO scenario [13], [21], [22], [23]. According to theory [21], [24] and real-world satellite experiments [13], [14], it is evident that the Doppler shift effect poses a challenge to the physical layer of LoRa receivers, often resulting in degraded communication performance due to high packet losses. Specifically, while the satellite link often benefits from line-of-sight (LOS) conditions in remote areas–allowing the channel to generally support a satisfactory link budget due to the high gain of satellite antennas [19], [20]–communication may still face challenges caused by the excessive Doppler effect [22]. As a result, there is a pressing need for effective strategies to mitigate the Doppler effect and thus enhance the performance of LoRa communications with LEO satellites.

In this paper, motivated by the massive deployment, as well as the high availability of real-world LoRa satellites data, we address this shortcoming by proposing a novel Doppler shift pre-compensation technique for LoRaWAN end devices. To the best of the authors' knowledge, this paper is the first study to propose a Doppler shift pre-compensation solution for LoRa DtS communication. The main contributions of this paper are summarized as follows:

- First, we propose a framework to modify existing LoRaWAN Class A operation which facilitates the reception of broadcast LoRa Doppler Beacons from LEO satellites. Specifically, we propose that the end device on Earth opens a receive window (RX0) before an uplink. During RX0, the end device receives a satellite beacon and processes it to estimate and pre-compensate for the Doppler shift in the subsequent uplink transmission.
- Second, we design a satellite beacon, termed Doppler Beacon, ensuring a short time-on-air duration to minimize the possible additional energy consumption by both the satellite and the end device receiver.
- Third, we validate the proposed framework using real-world LoRa satellites telemetry data from the TinyGS[1] platform. Our results confirm that the proposed framework increases the effective duration of the LEO satellite visibility window.
- Fourth, we investigate the impact of the proposed framework on the end device's battery lifetime as a function of the number of symbols in the Doppler Beacon and compare it with legacy LoRaWAN operations.

To facilitate the technical understanding of our framework, we make the developed simulator openly accessible (available from GitHub via [25]), supporting the research community to build upon it for future studies.

This paper is organized as follows. Section II provides fundamental background information. In Section III, we discuss relevant works addressing the impact of the Doppler effect on LoRa DtS communications and some state-of-the-art Doppler shift pre-compensation solutions for satellite systems. Section IV introduces the proposed Doppler shift pre-compensation technique. In Section V, we present the real-world LoRa satellites dataset. Section VI presents the network configuration and discusses the results illustrating the potential of our idea. Section VII discusses future research directions. Finally, Section VIII summarizes our conclusions.

II. TECHNICAL BACKGROUND

To lay the foundation for the proposed Doppler shift pre-compensation scheme, this section presents the technical background. Table 1 presents the key terminologies along with their definitions.

A. SATELLITE AND EARTH GEOMETRIC MODEL

This paper assumes a typical circular orbit and takes the work in [26] as a basis to model a LEO satellite pass. A satellite in low Earth orbit is essentially in continuous free fall towards Earth. However, because of its high tangential velocity [11], as it falls, the curvature of the Earth causes the surface to recede away at the same rate, keeping the satellite in orbit rather than crashing to the ground. This creates a state of perpetual free fall around the planet. In an ideal circular orbit, the angular speed of a satellite is constant given by,

$$\omega = \sqrt{\frac{\mu}{a^3}}, \tag{1}$$

where $\mu = 3.986 \times 10^{14}$ m^3/s^2 is the Earth's standard gravitational parameter and $a = h + R_e$ (with h being the altitude above mean sea level and $R_e = 6371$ km the average Earth radius) denotes the radius of an imaginary spherical shell, which reflects the circular orbit of a LEO satellite around the center of the Earth as in Fig. 1.

[1] TinyGS (https://tinygs.com/).

TABLE 1. Key terms and their corresponding definitions.

Term	Definition
Acquisition-of-Signal	The point at which a satellite becomes visible to an end device.
Doppler shift	A significant frequency offset in the transmitted signal caused by the LEO satellite mobility.
Doppler rate	The change of the Doppler shift over time.
Loss-of-Signal	A point until which a satellite remains visible to the end device before disappearing from view.
Frequency Error Indicator	A LoRa built-in function that allows the end device to measure the frequency difference between the receiver's carrier frequency (set by the local oscillator) and the carrier frequency of the incoming LoRa signal.
TIANQI-7	A LoRa satellite which continuously broadcasts packets every 15 seconds.
TinyGS	A LoRa's Largest Open Source Global Satellite Network. It is a network of ground stations that receive LoRa packets from satellites.

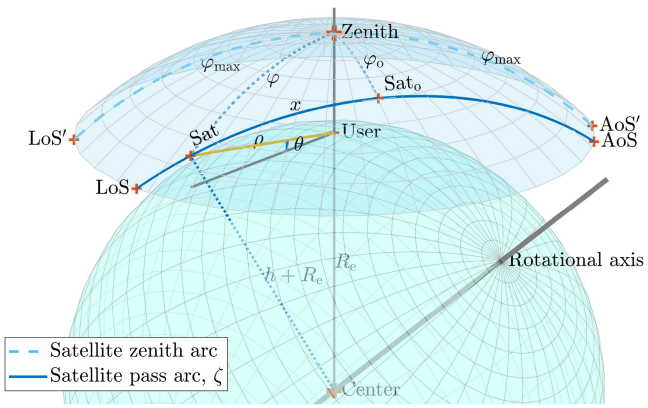

FIGURE 1. The satellite-to-end device (ground user terminal) basic geometry [26], indicating the elevation angle θ.

1) VISIBILITY WINDOW

To characterize a passing satellite trajectory, it is essential to understand the DtS geometry (between a user end device and an LEO satellite) depicted in Fig. 1. A satellite becomes visible to an end device at the Acquisition-of-Signal (AoS) point and remains visible until it reaches the Loss-of-Signal (LoS) point, where it disappears from view. Due to its fast mobility relative to the Earth's surface, it is only visible to a terrestrial end device when it enters the device's field-of-view (FoV), which has a span angle of $2\varphi_{max}$ measured from the Earth center (see Fig. 1). Consequently, during a pass, the satellite will always have an Earth-centered zenith angle $0 \leq \varphi \leq \varphi_{max}$, where $\varphi_{max} = \arccos(\frac{R_e}{a})$ [27]. Fig. 1 also highlights another important parameter, namely $\mathbf{Sat}_o$, which is the position of the satellite in its closest approach to the user and serves as the reference point for time $t = 0$.

The angular measure ζ of the pass arc can thus be calculated using the spherical triangle defined by the three points **AoS**, **Zenith**, and $\mathbf{Sat}_o$ as follows [26],

$$\zeta = 2\arccos\left(\frac{\cos\varphi_{max}}{\cos\varphi_o}\right), \tag{2}$$

where φ_o represents the zenith angle of the satellite at the closest approach point (see Fig. 1). This key parameter defines a satellite pass geometry concerning a terrestrial end device.

2) SLANT RANGE

The distance between the end device and the satellite, known as the slant range, varies over time t [26]. Given the satellite, end device, and Earth center geometry illustrated in Fig. 1, the slant range is calculated as,

$$\rho(t) = \sqrt{a^2 + R_e^2 - 2aR_e\cos\varphi_o\cos\omega t} \tag{3}$$

where t, in seconds, indicates the time corresponding to the position of the satellite along its trajectory during the visibility window. Then $-\frac{\tau}{2} \leq t \leq \frac{\tau}{2}$, where $\tau = \frac{\zeta}{\omega}$ denotes the duration of the visibility window. One can find the elevation angle θ from ρ as [21]

$$\theta(t) = \sin^{-1}\left(\frac{h^2 + 2hR_e - \rho(t)^2}{2\rho(t)R_e}\right). \tag{4}$$

B. DOPPLER EFFECT

The amount of Doppler shift varies over time within the satellite's visibility window $-\frac{\tau}{2} \leq t \leq \frac{\tau}{2}$ [11]. This phenomenon is due to the temporal variation in the slant range ρ, which changes the relative velocity between the end device and the satellite, thus introducing a Doppler shift. Specifically, the Doppler shift experienced by the end device/satellite is given by

$$f_d(t) = -\frac{v(t)}{c}f_c, \tag{5}$$

where $v(t)$ is the relative velocity[2] of the satellite as seen by an end device, f_c is the carrier frequency, and c denotes the speed of light.[3] Following the slant range ρ and the relative time t, one can find the relative velocity $v(t)$ by $\frac{d}{dt}\rho(t)$ [26].

The Doppler rate, which denotes the rate of change of the Doppler shift over time, is calculated as $\Delta f_d(t) = \frac{d}{dt}f_d(t)$. It has been proven that both the Doppler shift and the Doppler rate can significantly degrade the performance of LoRa DtS communications, primarily by causing frequency synchronization loss, which leads to increased packet losses [11], [13], [21].

[2] $v(t)$ is assumed to be negative, thus generating a positive Doppler shift, when the satellite is moving toward the end device. Conversely, if the satellite is moving away from the end device, $v(t)$ will be positive, resulting in a negative Doppler shift.

[3] Equation (5) provides a good approximation of the Doppler shift when $v(t)$ is small compared to c, which holds true in all practical cases.

C. LORA MODULATION

Here, we present the fundamental principles of LoRa, which is based on the chirp spread-spectrum (CSS) modulation [8], [21]. In particular, the basic waveform of LoRa is a linear chirp (symbol). A LoRa chirp is a sinusoidal signal whose frequency varies linearly over time within a specified bandwidth. Given the basic chirp, multiple parameters determine the LoRa waveform, namely the bandwidth $B \in \{31.25, 62.5, 125, 250, 500\}$ kHz, the spreading factor $\mathrm{SF} \in \{7, 8, 9, 10, 11, 12\}$, the cardinality of the modulation alphabet $M = 2^{\mathrm{SF}}$, and the chirp duration T_c, chosen such that $BT_c = M$.

For a configured SF, the LoRa transmitter has $M = 2^{\mathrm{SF}}$ different chirp options. Each chirp is a unique symbol that is uniquely mapped to one of the M symbols within the modulation alphabet set, $\mathcal{S} = \{0, 1, 2, \ldots, M-1\}$.

In particular, these M chirps are different, each starting from a distinct initial frequency. These starting frequencies are regularly spaced with a step size of $\Delta f = \frac{B}{M}$ Hz [8]. For a given bandwidth B, the frequency step size Δf is significantly smaller for higher SFs than for lower SFs. This makes higher SFs more vulnerable to the Doppler effect.

LoRa offers the low data rate optimization (LDRO) feature to combat the Doppler effect, increasing the frequency separation between chirps by decreasing the number of bits per symbol by two. Specifically, LDRO reduces the modulation alphabet to $M = 2^{(\mathrm{SF}-2)}$ and consequently increases the frequency separation between chirps by four times. This way, LoRa LDRO improves the robustness to the Doppler rate. However, this improvement comes at the cost of a reduced data rate and a lower spectral efficiency.

Remark: In the following, we will distinguish between the bandwidth of the downlink signal (propagating from the satellite to the end device), denoted as B_{downlink}, and the bandwidth of the uplink signal, referred to as B_{uplink}. In fact, we will assume that different bandwidths are used for the uplink and downlink to better match the specific characteristics of each link, with the downlink supporting Doppler estimation and the uplink dedicated to data communications.

D. LORA DOPPLER TOLERANCE

According to the Semtech LoRa product datasheets [28], [29], the application notes on crystal oscillator selection [30] and Doppler immunity [31], as well as validation through real-world flight tests [13], LoRa receivers can tolerate Doppler shifts of up to $f_{\mathrm{static}} = \pm 25\%$ of the signal bandwidth B [14], [21], at the time of signal reception. Specifically, a transmitted LoRa packet is lost if the Doppler shift in the channel exceeds f_{static}. During a packet reception, the Doppler rate causes variations in the carrier frequency of an incoming packet. To successfully demodulate a LoRa packet, it is also required that the change in carrier frequency of an incoming packet during reception must also not exceed a given threshold f_{rate} [21]. Table 2 shows the LoRa Doppler tolerance thresholds for different families of transceivers, where $L = 16$ when LDRO is enabled, and $L = 1$ otherwise.

TABLE 2. LoRa Doppler shift and Doppler rate tolerance limits.

Transceiver Model	Doppler shift (f_{static})	Doppler rate (f_{rate})	Reference
LR11xx, SX1302	$\pm 0.25 \times B$	$\frac{0.1 \times B}{2^{\mathrm{SF}}}$ Hz/symbol	[31]
SX12xx, SX1301	$\pm 0.25 \times B$	$\frac{L \times B}{3 \times 2^{\mathrm{SF}}}$ Hz/packet	[32]

E. LORA BUILT-IN FREQUENCY ERROR INDICATOR

LoRa transceivers are equipped with the capability to measure the Doppler shift that affects the received signal using the Frequency Error Indicator (FEI) function. A successful FEI operation requires two conditions [28]:

- *Condition I:* FEI measurement must have started during the reception of the incoming signal preamble.
- *Condition II:* The frequency deviation must not exceed the f_{static} threshold in Table 2. Otherwise, the spectrum of the received signal will fall, at least partially, outside the passband of the receive filter.

III. RELATED WORKS

This section discusses laboratory experiments, satellite flight-test measurements, and theoretical works that examine the impact of the Doppler effect on LoRa DtS performance. Additionally, we present some state-of-the-art countermeasures to combat the Doppler effect and associated relevant challenges.

A. ANALYSIS OF THE DOPPLER EFFECT ON LORA

According to the Doppler effect model presented in Section II-B, the magnitude of the Doppler shift reaches its maximum at the beginning and the end of the satellite's visibility window ($-\frac{\tau}{2} \leq t \leq \frac{\tau}{2}$), when, conversely, the magnitude of the Doppler rate reaches its minimum.

In such conditions, the carrier frequency of the received signal deviates significantly from the carrier frequency of the transmitted signal [13], [21], although the variations are relatively slow. In contrast, the Doppler shift is at its minimum for elevation angles where the satellite is closest to the end device, while the Doppler rate attains its maximum.

In existing state-of-the-art, several research methods, including theoretical investigations [21], laboratory [22], [23] and real-world satellite experiments [13], [14] have been used to understand the reliability of LoRa DtS communications under Doppler effect. In [23], laboratory tests aim to understand the impact of the Doppler effect and to evaluate the feasibility of direct LoRa communication between a terrestrial end device and a LEO satellite. These experiments use a radio frequency vector signal generator to synthesize and transmit a LoRa signal. On the receiver end, a LoRa transceiver from the Semtech SX1278 family was used. The channel accounts for the Doppler effect characteristics corresponding to the 430 MHz carrier frequency and a satellite orbital height of 200 km. The authors further

extended this activity in [22] and evaluated the feasibility of direct communication between a LoRa end device and a LEO satellite accounting for Doppler shifts corresponding to carrier frequency of 434 MHz, 200 km and 550 km orbital heights.

Following these activities [22], [23], in September 2020, a LoRa LEO satellite named Norby was launched, equipped with a SX1278 transceiver on-board. It is orbiting at the height of 560 km and operating at the carrier frequency of 436.7 MHz [14]. More recently, a second-generation satellite, Norby-2, was launched on June 27, 2023. The Norby flight testing experiments and results presented in [13] provided a foundational understanding of the limitations of LoRa DtS in real-world scenario. Similarly to the results in [22], [23], the experimental results in [13] confirmed that the Doppler effects may lead to packet losses in the LoRa DtS scenario. These studies complement each other, concluding that Doppler shift and rate affect LoRa communication performance at different elevation angles [13], [21], [23]:

- The Doppler shift prevents communication when it exceeds a threshold f_{static}. This typically occurs at the beginning and end of the visibility window, corresponding to the maximum link distance.
- The Doppler rate causes packet losses and prevents communication when exceeding the threshold f_{rate}. This typically occurs when the satellite is closest to the zenith, i.e., at its highest elevation angle.

Moreover, concerning LoRa DtS communication at 868 MHz, laboratory experiments have been conducted using software-defined radio (SDR) devices to emulate the Doppler effect in a LoRa satellite link, focusing on a specific set of communication parameters [33]. Similarly to the results in [13], [22], [23], the SDR-based results confirmed that LoRa DtS links are vulnerable to the Doppler effect.

Recently, orthogonal time frequency space (OTFS) and affine frequency division multiplexing (AFDM) have emerged as important waveforms that benefit from the Doppler diversity and offer highly reliable communication in highly mobile scenarios [34], [35]. As in LoRa, AFDM is a technique based on chirp signals. However, further research will be required to study how DtS communication can benefit from Doppler diversity.

B. DOPPLER SHIFT PRE-COMPENSATION: OPTIONS AND CHALLENGES

It is worth emphasizing that the above-mentioned studies do not propose any countermeasure against the Doppler effect in LoRa DtS [13], [21], [22], [23]. Indeed, Doppler shift compensation for LoRa DtS communication has received little attention in the literature. In [24], a LEO satellite receiver architecture is designed to combat the Doppler shift, which is further validated using simulations. In [36], a scheme is proposed that adds pilot signals to the payload during packet transmission to estimate and compensate the Doppler shift at the receiver end. Using these known pilots, the receiver estimates the Doppler shift and rate at the satellite. However, these additional pilots resulted in a 33.33% increase in the packet size, which increases the energy consumption and could raise interference issues.

Other solutions inspired by techniques for other wireless technologies can be investigated for LoRa DtS. To address the Doppler effect challenge in 5G Non-Terrestrial Networks (NTN), 3GPP specifies that an end device must have a Global Navigation Satellite System (GNSS) module. The satellite broadcasts ephemeris[4] information to assist the end device in Doppler shift pre-compensation. Before an uplink, the 5G NTN end device uses GNSS to measure its location and the ephemeris information to calculate and pre-compensate for the Doppler shift [37], [38].

Motivated by the 3GPP NTN solution, one may develop a Doppler shift pre-compensation scheme where the LoRaWAN end device has GNSS capabilities [39], [40] and the LoRa satellite broadcasts its ephemeris information which includes the state vector (position and velocity) in a given future time frame. A LoRaWAN end device could then calculate and pre-compensate the Doppler shift using its location and satellite ephemeris information. However, this approach comes with several downsides:

- Primary motivations for development of LoRa DtS technology are the low cost and energy efficient connectivity [11], [19], [20], [41]. Notably, integrating GNSS into LoRaWAN end devices would increase their cost. The frequent GNSS measurements and position fix would also increase energy consumption and reduce battery life [37], [39]. In [39], the study reports that the GNSS module consumes approximately up to 67% of the total energy of a LoRaWAN end device.
- GNSS signals are weak due to large path loss, not ubiquitous, and vulnerable to interference and spoofing [37], [38]. Any inaccuracy in GNSS measurements could cause errors in Doppler shift pre-compensation. Note also that, for the next generation DtS, recent research suggests that end devices should be capable of operating successfully without relying on a GNSS module [42].
- After obtaining GNSS measurements, the end device can open an additional receive window to acquire satellite information, which may include positional data derived from two-line element (TLE) data [5] or ephemeris. In the case of TLE, 138 ASCII characters encode the orbital information, resulting in a payload of 138 bytes. The ephemeris data are typically much longer than TLE. To transmit such data from the satellite to end devices, the LoRa frame structure adds coding, header, and cyclic redundancy check (CRC) bits, thereby

[4]An ephemeris is a table that provides positional (and optionally velocity) information about a satellite over a specified period of time.

[5]TLE is a data format used for encoding the orbital elements of an Earth-orbiting object defined at a specific time. The state (position and velocity) of a satellite at any point in the near past or near future can be predicted with some accuracy from TLE with an orbit propagator. Notably, TLE-based estimations of a satellite's position and velocity are less accurate than those derived from ephemeris data.

increasing the overall payload. Consequently, the end device would have to open a receive window for a long time, increasing energy consumption [43].

- Due to the satellite's orbital propagation, predicting its location based on the ephemeris or TLE is a computationally demanding operation. In the case of TLE data, the accuracy of the Doppler shift pre-compensation depends on several factors, including (i) Accuracy and freshness of TLE data; (ii) Accuracy of the end device local clock; (iii) Accuracy of the orbit propagator Doppler shift theoretical estimation; (iv) Accuracy of the GNSS measurement performed by the end device. Any mismatch in one of these could affect the Doppler shift estimation and pre-compensation accuracy.

Notably, LoRa LEO satellites are designed to support a massive number of end devices, which presents a significant challenge for the satellites in compensating for the Doppler shift. Given the limited energy and computational resources available at the satellite, this paper addresses the Doppler shift by implementing pre-compensation at the transmitter side, thereby avoiding any additional processing burden on the receiver.

IV. PROPOSED METHOD

This paper introduces a GNSS-independent solution for Doppler shift pre-compensation in LoRa DtS communications. We propose that a satellite broadcasts a short Doppler Beacon, which contains no payload, header and CRC bits. The end device needs to receive a single Doppler Beacon in the downlink to estimate and pre-compensate for the Doppler shift in the subsequent uplink communication. This scheme increases the satellite receiver's capability to successfully demodulate the incoming uplink LoRa signals. It is worth observing that increasing robustness to the Doppler shift also increases the duration of the satellite's effective visibility window, as communication becomes possible for lower elevation angles.

Regarding the Doppler rate, the immunity threshold depends on the family of transceivers being used.

As shown in the third column of Table 2, achieving immunity to the Doppler rate is primarily possible by increasing the bandwidth and reducing the SF. It is worth noting, however, that according to the Application Note [31], for an orbital height of 500 km, the LR11xx, SX1302 families of transceivers working at 400 MHz ensure immunity to the Doppler rate even with a bandwidth as low as 125 kHz and SFs from 7 to 11. This observation motivated us to focus primarily on the Doppler shift, leaving the Doppler rate to future work. For a comprehensive investigation on LoRa DtS communications, additional analyses on link budget and interference impact can be added on top of the investigation presented in this paper, in line with [19], [20], [41].

Concerning the classes of LoRa receivers, earlier studies on LoRa DtS communications advocate for the use of Class A end devices and assume that communication occurs exclusively in the uplink direction, without receiving time-synchronization beacons from satellites [11], [19], [20], [41], [44], [45]. Only a few studies explore using Class B end devices for DtS connectivity [46], [47]. To align with most existing literature, we adopt LoRaWAN Class A end devices as the baseline scenario for developing and validating the Doppler shift pre-compensation strategy presented in this work. Nevertheless, Section VII discusses the potential and challenges that may arise when considering Class B and Class C end devices in this framework.

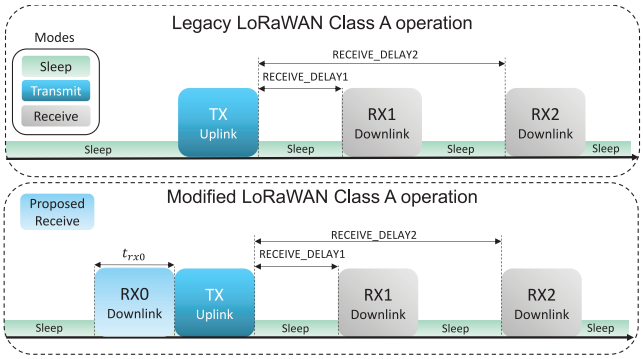

FIGURE 2. Basic operation of legacy and proposed LoRaWAN Class A.

Remark: Table 2 shows that increasing the bandwidth makes the receiver more resilient to Doppler effects. On the other hand, larger bandwidths are detrimental to the link budget due to the increased noise that enters the receiver. These conflicting aspects suggest that different bandwidths, namely B_{uplink} and B_{downlink}, could be adopted in the two directions, leveraging the fact that the uplink and downlink have different requirements, as it is explained in the following section.

A. PROPOSED MODIFICATION FOR LORAWAN CLASS A

We assume that a LoRa LEO satellite continuously broadcasts Doppler Beacons toward Earth. The inter-arrival time between two consecutive Doppler Beacons is considered negligible, effectively approaching zero. As a result, each Doppler Beacon is followed by an identical Doppler Beacon without any delay between the two consecutive beacon transmissions. Any end device within the satellite's coverage area can receive the Doppler Beacons, provided it opens a receive window.

Based on this assumption, we propose a modified LoRaWAN Class A operation, where the end device opens an additional receive window (RX0), having an adequately chosen duration t_{rx0}. Fig. 2 shows the legacy and proposed Class A operation, whereas Fig. 3 presents a high-level illustration of (a) the considered network scenario, (b) the components of the satellite Doppler Beacon, and (c) the steps involved in our proposed method.

Specifically, before initiating an uplink transmission, an end device transitions from sleep mode to receiving mode

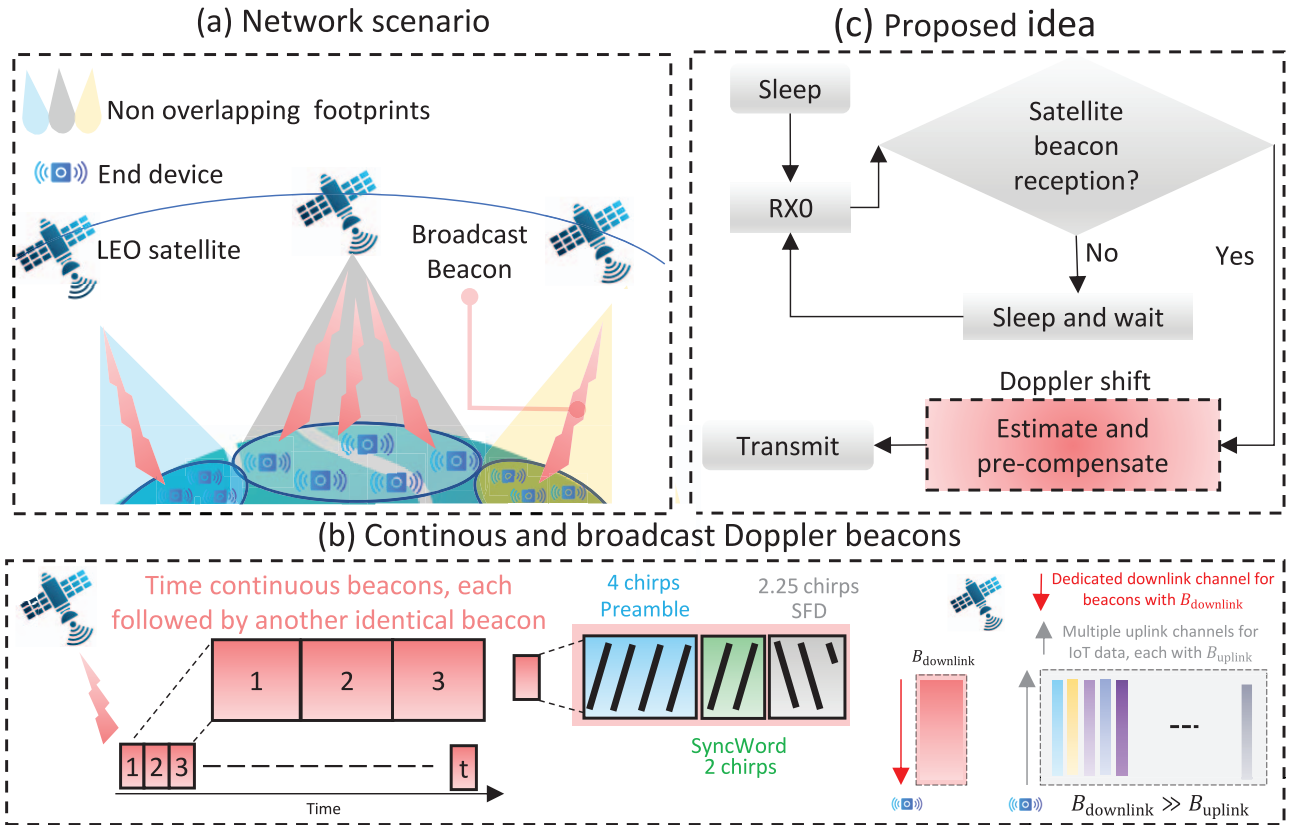

FIGURE 3. The high-level illustration of the (a) considered network scenario; (b) components of Doppler Beacon broadcast by satellite; and (c) proposed Doppler shift estimation and pre-compensation scheme.

by opening the RX0 window. This RX0 mode allows an end device to listen to a predetermined downlink frequency channel and receive a Doppler Beacon from a visible satellite. If the end device receives the Doppler Beacon, it estimates the Doppler shift using the LoRa built-in FEI function [28] introduced in Section II-E. The end device uses this estimation to pre-compensate the Doppler shift by properly shifting the uplink carrier frequency in the opposite direction.

Next, the end device transmits a Doppler shift pre-compensated signal toward the satellite, as shown in Fig. 2 and Fig. 3. After the uplink transmission, the end device opens the regular Class A receive windows, RX1 and RX2. The default delay for RX1, often called RECEIVE_DELAY1, is a network parameter detailed in the LoRaWAN Regional Parameters document published by the LoRa Alliance®. After RX1 closes, the end device introduces a one-second delay, RECEIVE_DELAY2, before opening RX2 [48].

Conversely, if the end device receives no Doppler Beacon signal during RX0, this indicates a LOS blockage or the absence of a visible satellite at that particular moment. In such cases, the end device reverts to sleep mode and waits for a predetermined interval (t_w) before repeating the process as illustrated in Fig. 3.[6] The duration of t_w depends on the nature of the IoT application.

B. DOPPLER BEACON DESIGN

We design the Doppler Beacon to ensure that the two LoRa's built-in FEI conditions, as outlined in Section II-E, are satisfied. This guarantees accurate estimation of the Doppler shift in the downlink RX0 window.

1) LENGTH

To simplify the design and ensure compatibility with LoRaWAN specifications, we propose that the satellite Doppler Beacon consists of the standard LoRa preamble without any header, payload, encoding, and CRC bits as illustrated in Fig. 3 (b). One of the primary reasons for avoiding the header, payload, and CRC is to minimize the beacon's time-on-air, thereby ensuring that the Doppler shift does not vary significantly during beacon reception and keeping the energy expenditure of the end device for

[6]Icons are made by afif fudin, Noplubery and Elzicon from www.flaticon.com.

demodulation as low as possible. The Doppler Beacon's time-on-air can be calculated as

$$t_{\mathrm{b}} = N\mathrm{sym} \times \frac{2^{\mathrm{SF}}}{B_{\mathrm{downlink}}}. \tag{6}$$

where Nsym is the number of symbols in a Doppler Beacon. In this work, we assume that the beacon comprises $N\mathrm{sym} = 8.25$ symbols, including (i) the preamble that comprises four upchirps, (ii) the synchronization word of two upchirps, and (iii) the start frame delimiter (SFD), consisting of two and a quarter downchirps symbols. This is the minimum number of symbols required for the successful detection of the Doppler Beacon [49].

2) KEY PARAMETERS

We assume that the satellite continuously transmits Doppler Beacons. To ensure their successful reception, we set the duration of the RX0 window to be twice the Doppler Beacon's time-on-air given by $t_{\mathrm{rx0}} = 2 \times t_{\mathrm{b}}$. This assumption effectively accounts for potential mismatches in Doppler Beacon scheduling, such as slight delays between consecutive transmissions that may introduce discontinuities in the Doppler Beacons. It is important to note that, despite having a sufficient link budget, the end device may fail to receive the downlink Doppler Beacon in RX0 if the Doppler shift affecting the beacon transmission exceeds the tolerance threshold f_{static} specified in Table 2. To prevent this issue, it is convenient to use a large enough bandwidth for Doppler Beacon transmissions, as this makes the end device more resilient to Doppler shifts (see Table 2).

Although large bandwidths can negatively impact the link budget due to increased noise entering the receiver, this should not be considered a significant issue, given that satellite transmissions have fewer constraints regarding transmitted power and antenna directivity compared to end devices, which are often battery-powered and limited in size. In the downlink, therefore, a larger bandwidth B_{downlink} can be selected to enable the end device to demodulate the beacon despite the Doppler shift and accurately estimate it in preparation for pre-compensating it in the subsequent uplink transmission.

Specifically, following Table 2 and given the maximum Doppler shift $\max(f_{\mathrm{d}})$, expected in the downlink channel, the appropriate bandwidth for the transmission of the Doppler Beacons must satisfy the condition

$$B_{\mathrm{downlink}} > 4 \times \max(f_{\mathrm{d}}). \tag{7}$$

3) ENERGY CONSUMPTION MODEL

This paper also evaluates the additional energy consumption associated with Doppler Beacon reception in RX0. We use a basic Class A energy profile based on the one presented by Semtech in [50]. Table 3 shows the operational states, their duration, and current consumption. Let $N_{\mathrm{states}} = 5$ be the number of states. Here, T_i and I_i represent the duration and current consumption of these states as given in Table 3. Then, the total average current consumption is given by

TABLE 3. A basic LoRa current consumption profile for different states, their duration, and average current consumption [50].

State no. i	State name	Duration T_i notation	Duration T_i millisecond	Current I_i notation	Current I_i mA
1	RX0	t_{rx0}	$2 \times t_{\mathrm{b}}$	I_{rx0}	11
2	TX	t_{tx}	refer to [28]	I_{tx}	32
3	RX1	t_{rx1}	$\frac{5\times 2^{\mathrm{SF}}}{B_{\mathrm{downlink}}}$	I_{rx1}	11
4	RX2	t_{rx2}	$\frac{5\times 2^{\mathrm{SF}}}{B_{\mathrm{downlink}}}$	I_{rx2}	11
5	Sleep	t_{sleep}	refer to [51]	I_{sleep}	0.001

$$I_{\mathrm{average}} = \frac{1}{T_{\mathrm{notification}}} \sum_{i=k}^{N_{\mathrm{states}}} T_i \times I_i, \tag{8}$$

where $T_{\mathrm{notification}}$ is the uplink reporting period of the IoT end device. For legacy LoRaWAN operation, the first state RX0 is absent. Therefore, $k = 1$ denotes a modified operation and $k = 2$ represents a legacy LoRaWAN operation. For a detailed description of the LoRa uplink time-on-air (t_{tx}) in Table 3, refer to Semtech datasheet in *Section 4.1.1.7. Time on air* of [28]. In Table 3, the total time spent by the end device in sleep mode is denoted as I_{sleep} as detailed in [51]. This energy consumption model assumes that the RX1 and RX2 reception durations are equivalent to 5 symbols as in [50]. The theoretical battery lifetime of operation is given by

$$T_{\mathrm{lifetime}} = \frac{C_{\mathrm{battery}}}{I_{\mathrm{average}}}, \tag{9}$$

where C_{battery} is battery charge expressed in mAh.

C. SATELLITE CONFIGURATION

For illustration purposes, we consider a LEO satellite mega-constellation that provides continuous coverage to end devices. Each LEO satellite has a single gateway, generating a single communication beam. Additionally, each satellite broadcasts identical Doppler Beacons. The coverage footprints of the satellites are non-overlapping [41], ensuring that Doppler Beacons are free from interference from beacons transmitted by other satellites. We assume that each LEO satellite is equipped with high-gain transmit and receive antennas to compensate for the path loss due to the large link distance. This ensures that DtS communication achieves a sufficient link budget for both the uplink and downlink channels. With ongoing technological advancements, it is increasingly feasible for LEO satellites to achieve such high gains, further supporting reliable communication. For example, AST SpaceMobile's satellite BlueWalker 3 features an antenna with an aperture of 693 square feet (64 m^2), offering up to 45.5 dBi gain [52].

D. END DEVICE CONFIGURATION

We assume a LoRa end device without GNSS capabilities, which can support our solution without requiring knowledge of its location. Notably, LoRa DtS end devices are usually battery-powered, which means they need to save as much energy as possible to provide a longer battery lifetime [11]. This also requires reducing the transmitted power to the minimum level needed to maintain a reliable link. Therefore, using a narrow bandwidth B_{uplink} is beneficial to enhance the signal-to-noise ratio at the satellite's receiver.

It is important to note that a narrow bandwidth is feasible despite the increased vulnerability to Doppler shift, thanks to the pre-compensation performed by the end device. Clearly, adopting a narrow bandwidth B_{uplink} reduces the data rate. This is the price to be paid to enable communications with low energy consumption and may not be a significant concern for low data rate IoT applications.

E. DOPPLER SHIFT ESTIMATION AND PRE-COMPENSATION

We propose that the end device leverages the LoRaWAN built-in FEI function (see Section II-E) for Doppler shift estimation.

Specifically, we assume that the end device opens RX0 at a time instant t within the satellite visibility window $-\frac{\tau}{2} \leq t \leq \frac{\tau}{2}$, and performs a FEI measurement on the received beacon, allowing it to estimate the Doppler shift $f_{\text{e}}(t)$ in the downlink. To avoid interference, we also assume that the downlink and uplink channels operate at different carrier frequencies, resulting in a slightly different Doppler profile for downlink and uplink depending on the channel spacing. Given the instantaneous FEI measurement in the downlink, the end device can thus pre-compensate for the Doppler shift in the uplink, while accounting for the difference between the downlink and uplink carrier frequencies as[7]

$$f'(t) = f'_{\text{c}} + f_{\text{e}}(t)\left(\frac{f'_{\text{c}}}{f_{\text{c}}}\right), \tag{10}$$

where f'_{c} and f_{c} are the uplink and downlink carrier frequencies, respectively. Notably, f'_{c} is the nominal uplink carrier frequency assigned to the communication link irrespective of the Doppler effect. The Doppler shift experienced by the uplink signal is thus

$$f'_{\text{d}}(t) = -\frac{v(t)}{c} f'(t). \tag{11}$$

V. REAL-WORLD LORA SATELLITES DATASET

This section discusses the real-world LoRa satellite telemetry dataset used in this paper, as well as the estimated Doppler shift and the theoretically predicted Doppler shift.

A. LORA FEI MEASUREMENTS: TINYGS DATASET

To assess the effectiveness of the proposed scheme, we used real-world LoRa satellite telemetry data accessed from the TinyGS dataset [15] on June 11, 2024, and February 15, 2025. These two dates, eight months apart, include both summer and winter seasons. Among the various TinyGS ground stations, we selected the W7RCS Console,[8] located in Burien, Washington, United States. One of the reasons for choosing W7RCS is its favorable propagation condition. As of July 8, 2024, and February 18, 2025, W7RCS has received 65,956 and 133,000 packets, respectively, from Earth-orbiting LoRa satellites.

From the available satellites, we selected TIANQI-7 and TIANQI-27 due to their more frequent packet transmissions (every 15 seconds) compared to other satellites. For example, the Norby satellite transmits a packet every 60 seconds [13]. TIANQI-7 operates at $f_{\text{c}} = 400.45$ MHz, $B_{\text{downlink}} = 500$ kHz and SF9. The orbital height of TIANQI-7 is $h = 518$ km. TIANQI-27 uses different parameters: $f_{\text{c}} = 400.265$ MHz, $B_{\text{downlink}} = 125$ kHz, SF10 and orbital height of $h = 904$ km. Notably, we calculated h for both TIANQI-7 and TIANQI-27 using MATLAB's Satellite Communications Toolbox based on their TLE data.[9] Table 4 compares these two satellites and lists the number of confirmed packets as of February 15, 2025.

TABLE 4. Comparison of TIANQI-7 and TIANQI-27 key parameters.

Parameter	TIANQI-7	TIANQI-27
Bandwidth (kHz)	500	125
Orbital Height (km)	518	904
Inclination (°)	97.5575°	44.9764°
Spreading Factor (SF)	9	10
Carrier Frequency (MHz)	400.45	400.265
Transmit power (mW)	9000	9000
Confirmed satellite packets	1,451,098	582,261
Launch Date	November 3, 2019	May 29, 2024

Let $F_{\text{P}} = \{F_{\text{P}}(1), F_{\text{P}}(2), F_{\text{P}}(3), \ldots, F_{\text{P}}(n)\}$ denote the set of discrete time theoretical Doppler shifts predicted using TinyGS's orbit propagator[10] that leverages the TLE set of TIANQI-7 and TIANQI-27. Similarly, let $F_{\text{E}} = \{F_{\text{E}}(1), F_{\text{E}}(2), F_{\text{E}}(3), \ldots, F_{\text{E}}(n)\}$ represent the corresponding set of estimated Doppler shifts measured by the TinyGS's end device using LoRa FEI on TIANQI-7 and TIANQI-27 packets. Every $F_{\text{E}}(i)$ in the set F_{E} corresponds to a $F_{\text{P}}(i)$ in the set F_{P}, where i ranges from 1 to n.

In this regard, the upper plot on the left-hand side of Fig. 4 shows both $F_{\text{P}}(n)$ and $-F_{\text{E}}(n)$, obtained from the W7RCS TinyGS [15] receiver during a single pass of TIANQI-7 on June 11, 2024. The upper plot on the right-hand side of

[7] The output of FEI $f_{\text{e}}(t)$ is always opposite to actual Doppler shift $f_{\text{d}}(t)$.

[8] https://tinygs.com/station/W7RCS@6500205772

[9] https://se.mathworks.com/products/satellite-communications.html

[10] An orbit propagator is a solver that calculates the position and velocity of an object whose motion is predominantly influenced by gravity from celestial bodies.

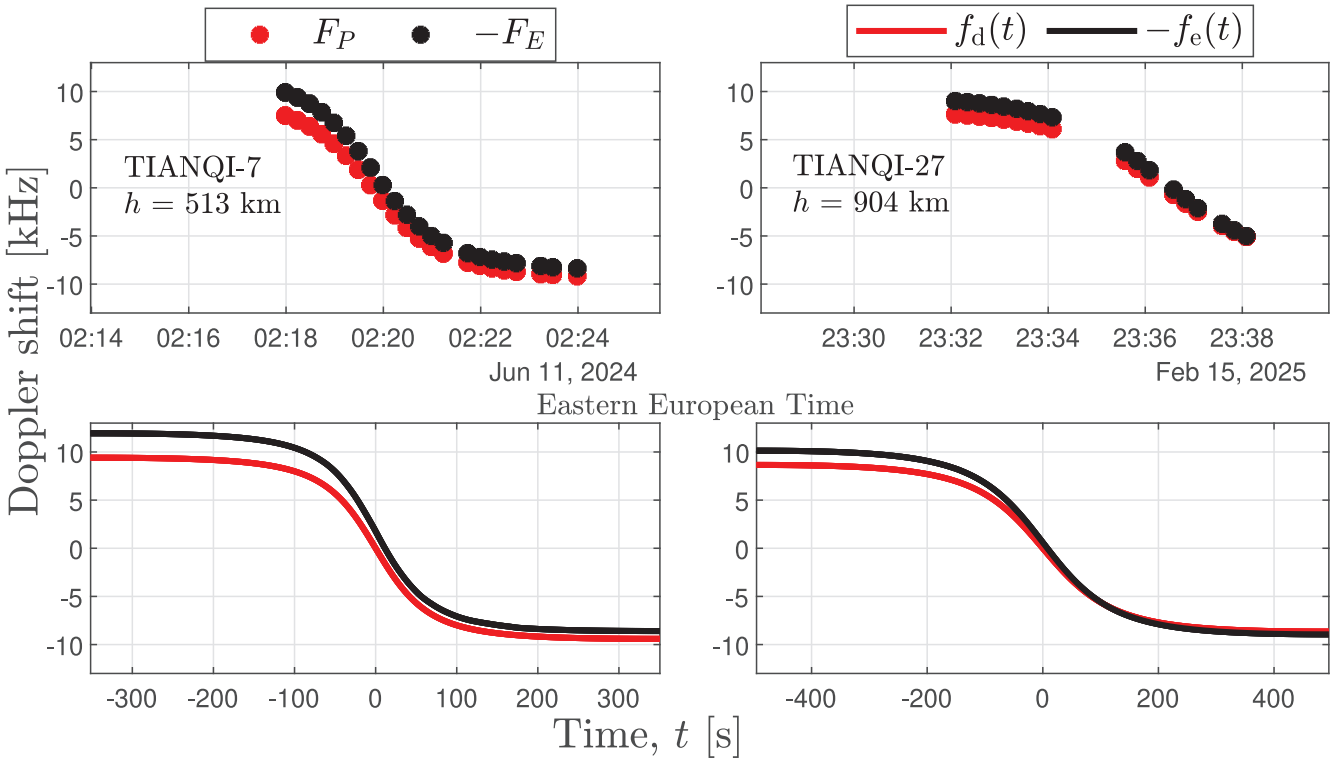

FIGURE 4. The left-hand side of this figure presents TinyGS data for a single pass of TIANQI-7 on June 11, 2024, while the right-hand side displays TinyGS data for a single pass of TIANQI-27 on February 15, 2025. The upper plot of the figure shows TinyGS's empirically estimated Doppler shift (F_E) and corresponding predicted Doppler shift (F_P). The lower plot shows extrapolated estimated Doppler shift f_e and corresponding predicted Doppler shift f_d.

Fig. 4 shows the same data for a single pass of TIANQI-27 on February 15, 2025. The discrete nature of these data points is evident (only the dots correspond to actual data).

Under ideal conditions, $F_E(i) = -F_P(i)$, as the FEI outputs the opposite of the Doppler shift. However, usually, there is a mismatch of a few kHz between $-F_E(i)$ and $F_P(i)$. The upper plot of Fig. 4 illustrate this mismatch between $-F_E(i)$ and $F_P(i)$, with TIANQI-7 exhibiting a slightly greater discrepancy compared to TIANQI-27. This mismatch is likely due to the following factors:

1) The use of outdated TIANQI-7 and TIANQI-27 TLE data by the TinyGS server for computing F_P using the orbit propagator;
2) Slightly inaccurate coordinates of the end device (W7RCS) used by the TinyGS server along with TIANQI-7 and TIANQI-27 TLE data for computing F_P;
3) Residual Doppler shifts caused by differences in the oscillators of both satellites (TIANQI-7 and TIANQI-27) and the end device (W7RCS);
4) The possibility of measurement error in LoRaWAN built-in FEI estimation which can further influence F_E.

It is worth emphasizing that the proposed Doppler shift pre-compensation scheme relies on a fresh estimation of $F_E(i)$, measured by the end device before each uplink transmission using the LoRa built-in FEI. Therefore, the mismatch between $-F_E(i)$ and $F_P(i)$ does not impact the performance or effectiveness of the proposed framework.

B. INTERPOLATED AND EXTRAPOLATED DATASET

Satellites in the TinyGS network transmit packets at regular intervals, meaning that end devices cannot perform Doppler shift measurements during the silent periods between transmissions. For example, the TIANQI-7 and TIANQI-27 satellites transmit a LoRa packet at 15-second intervals [15], as clearly evident in the upper plots of Fig. 4.[11] Therefore, the F_E data from TinyGS satellites is discrete. Moreover, the experimental data does not cover the entire visibility window, as indicated by the asymmetrical behaviour of both $F_E(n)$ and $F_P(n)$ in Fig. 4.

Ideally, during a complete pass where $\varphi_o = 0$, the Doppler shift should reach zero when the elevation angle θ is 90°, indicating that the satellite is at Zenith. In such a pass, the Doppler shift would exhibit symmetrical behavior as the satellite approaches the end device (from AoS to Zenith) and then moves away (from Zenith to LoS). The asymmetry of both $F_E(n)$ and $F_P(n)$, as shown in the upper section of Fig. 4, clearly indicates that data is missing, particularly at the beginning of the visibility window. This could be due to several reasons: (i) reception failures caused by strong Doppler effects; (ii) reception failures caused by

[11]The upper plot of Fig. 4 also allows us to observe the absence of some dots, due to reception failures.

high path loss and shadowing; (iii) satellite pass trajectory corresponding to $\varphi_o \gg 0$.

However, to demonstrate the effectiveness of our pre-compensation methodology, we require the output of the FEI function for each elevation angle $0 \leq \theta \leq 90°$ within the visibility window. To address the data gaps and generate Doppler shift data for other f_c', f_c, B_{downlink} and h values, we used MATLAB's `interp1` function to compute the interpolated and extrapolated[12,13] estimated Doppler shift $f_e(t)$ representing the downlink channel. This function provides a finer sampling rate compared to F_E and applies to the satellite's entire visibility window $-\frac{\tau}{2} \leq t \leq \frac{\tau}{2}$. This step effectively addresses the sparse and incomplete nature of the TinyGS empirical data shown in the upper plots of Fig. 4.

Specifically, to generate $f_e(t)$, we used the following MATLAB example command: f_e = `interp1`(F_P, F_E, f_d, `'linear'`, `'extrap'`), where F_E represents the dependent variable and F_P is the independent variable. Notably, f_d corresponds to the theoretical Doppler shift in downlink channel for $-\frac{\tau}{2} \leq t \leq \frac{\tau}{2}$, which encompasses the entire visibility window. The interpolated and extrapolated f_e data illustrated in the bottom section of Fig. 4 follows the same trend as TinyGS empirical data F_E shown in the upper plots of Fig. 4. The interpolation and extrapolation procedure described above allowed us to obtain the values expected from the FEI function across the entire visibility window with fine granularity, which effectively provides $f_e(t)$.

Similarly, it is important to note that while the Doppler shift in the uplink signal, $f_d'(t)$ (11), is theoretically accurate, it does not account for the observed mismatch between $F_E(n)$ and $F_P(n)$, nor does it fully reflect empirical behavior. To better approximate the empirical behavior and account for this mismatch, we interpolate and extrapolate $f_d'(t)$ using TinyGS's data. Therefore, f_e' is representative of the Doppler shift $f_d'(t)$ experienced by the receiver onboard the satellite. As a result, the satellite receives the uplink signal frequency at

$$f_r'(t) = f'(t) - f_e'(t). \tag{12}$$

At a given time t, the actual Doppler shift experienced by a satellite is calculated as the difference between the nominal uplink carrier frequency f_c' and the received frequency f_r' representing the frequency at which the uplink signal arrives at the satellite.

[12]Interpolation allows us to fill the gap between adjacent measurements, whereas extrapolation generates values beyond the range of known measurements.

[13]We use the TinyGS FEI dataset and extrapolation only to validate the effectiveness of the proposed pre-compensation framework for each elevation angle $0 \leq \theta \leq 90°$ within the visibility window. It is important to note that these steps are not integral components of the proposed framework itself.

TABLE 5. Key notations and parameters for downlink (DL) and uplink (UL).

Notation	Parameter descriptions	Value
R_e	Earth average radius	6371 km
h	Satellite altitude	$200 - 10000$ km
a	Satellite orbit radius	$R_e + h$
φ	Earth centered zenith angle	-
φ_o	φ at the closest approach	$0°$
θ	Elevation angle	$0° - 90°$
$\theta_{\min}$	Minimum elevation angle	$0°$, $40°$
B_{downlink}	DL channel bandwidth	500 kHz
f_c	DL carrier frequency	400.45 MHz
f_d	DL channel Doppler shift	-
F_P	DL TinyGS predicted Doppler shift	-
F_E	DL TinyGS estimated Doppler shift	-
f_e	DL extrapolated version of F_E	-
B_{uplink}	UL channel bandwidth	$31.25, 62.5, 125$ kHz
f_c'	UL carrier frequency	$401.45, 868$ MHz, 2 GHz
f_d'	UL channel Doppler shift	-
f'	UL pre-compensated carrier frequency	-
f_e'	UL extrapolated version of F_E	-
f_r'	UL signal received frequency at satellite	-
f_{static}	LoRa Doppler shift tolerance	$\pm 0.25 \times B$

VI. NETWORK CONFIGURATION AND RESULTS

This section introduces the scenarios and key communication parameters used to validate the proposed Doppler shift pre-compensation framework and presents numerical results to assess its effectiveness. Table 5 lists the key notations along with their descriptions and values.

TIANQI-7 orbits at $h = 518$ km, which is a typical height for LEO and IoT satellites. Therefore, we opted for TIANQI-7 to validate our proposed framework. Given the TIANQI-7 B_{downlink}, the Doppler shift tolerance threshold $f_{\text{static}} = \pm 0.25 \times B_{\text{downlink}} = \pm 125$ kHz is high. Since the maximum Doppler shift experienced by TIANQI-7 downlink channel at $f_c = 400.45$ MHz is approximately 10 kHz, significantly lower than $f_{\text{static}} = 125$ kHz, it is highly unlikely that TIANQI's communications will suffer from Doppler shift in the downlink. This ensures the end device receives the beacon correctly, allowing it to accurately estimate the Doppler shift in preparation for the pre-compensation applied during uplink transmission.

On the other hand, to improve the link budget in the uplink – a critical aspect for battery-powered end devices – we assume that the end device shall transmit with a smaller bandwidth B_{uplink} which, however, makes it more susceptible to the Doppler shift effect. This is where our pre-compensation scheme comes into play,

making uplink transmission robust against Doppler effects despite the reduced bandwidth. To validate our Doppler shift pre-compensation scheme, we make the following assumptions:

- The satellite can simultaneously transmit Doppler Beacons on the downlink and receive packets from end devices on the uplink. This can be achieved using separate frequency bands for the two links. The satellite broadcasts Doppler Beacons on a predetermined frequency channel, which the end device monitors during RX0. The end device may select either a random or a dedicated pre-configured channel for transmission. In this paper, we assume $f_c = 400.45$ MHz for downlink. We use $f_c' = 401.45$ MHz, 868 MHz and 2 GHz for uplink. The latest LoRaWAN end devices support the S-band for satellite IoT connectivity. This motivated us to validate our framework also at $f_c' = 2$ GHz.
- We consider an extreme pass, in which the satellite directly passes over the end device, and the elevation angle θ between the end device and satellite reaches 90°, so that $\varphi_o = 0°$. The proposed method is also valid for other scenarios.
- The LEO satellite operates with $B_{\text{uplink}} = 31.25, 62.5,$ 125 kHz, $h = 200, 518$ km and $\theta_{\min} = 0°$ resulting in $\max(f_d') \approx 10$ kHz. It is noteworthy that some existing real-world LoRa satellites, e.g., Norby [13], also use $B = 31.25$ kHz.
- To successfully estimate this Doppler shift in RX0, and to remain consistent with TIANQI-7, we set $B_{\text{downlink}} = 500$ kHz to ensure that the condition expressed in (7) is met.

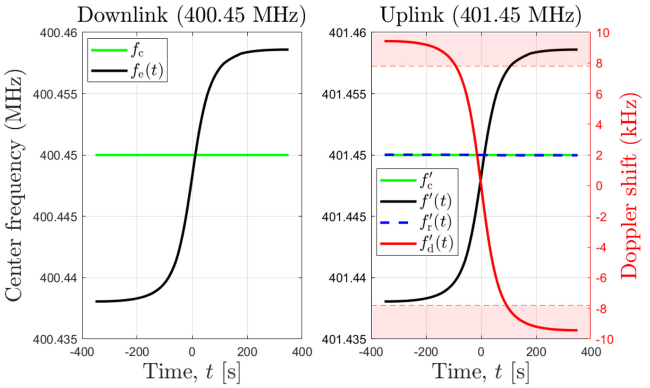

FIGURE 5. Effectiveness of proposed Doppler shift pre-compensation scheme for $B_{\text{uplink}} = 31.25$ kHz and $h = 518$ km. The left-hand side of the figure shows the carrier frequency f_c and FEI estimate f_e in the downlink channel. The right-hand side of the figure shows the pre-compensated uplink carrier frequency f' at the time of transmission and uplink signal carrier frequency f_r' when received by satellite.

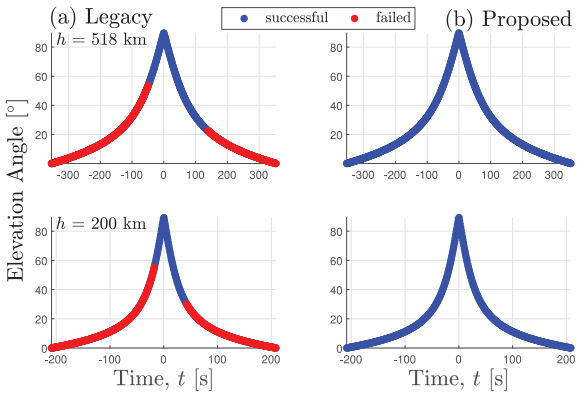

FIGURE 6. Comparison of LoRa DtS packet losses due to Doppler shift at $h = 518$ km and $h = 200$ km for $f_c' = 401.45$ MHz and $B_{\text{uplink}} = 31.25$ kHz, without (legacy) and with the proposed pre-compensation scheme. The upper part of the figure shows results for an LEO satellite orbiting at $h = 518$ km and the lower part of the figure reveals results for a VLEO satellite at $h = 200$ km.

A. VALIDATION OF THE PROPOSED PRE-COMPENSATION SCHEME

As illustrated in Fig. 3, the proposed solution uses the built-in FEI function to estimate the Doppler shift in the downlink and then uses the estimate to pre-compensate for the Doppler shift in the uplink. To validate the proposed Doppler shift pre-compensation, we use the network configurations discussed in Table 5. Specifically, we assume $B_{\text{uplink}} = 31.25$ kHz which results in $f_{\text{static}} = 7.8$ kHz. Without the pre-compensation, the uplink packet would be lost when $f_d' > f_{\text{static}}$, as marked by the red region in Fig. 5. With the proposed pre-compensation scheme, the incoming signal frequency $f_r' = 401.45$ MHz is the same as the configured uplink carrier frequency $f_c' = 401.45$ MHz, allowing the satellite to receive the packet successfully. It confirms the feasibility of our idea.

B. PACKET LOSSES

Next, we use the LoRa DtS analytical framework in [21] to investigate packet losses due to Doppler shift across different communication parameters, both with and without our pre-compensation scheme. This analysis focuses solely on packet losses caused by the Doppler effect. The model considers only a single end device with no co-channel interference. Additionally, it does not consider the channel link budget and assumes that the signal is sufficiently strong to reach an LEO satellite in orbit assuming reasonably high satellite antenna gains. The work in [21] concludes that satellite orbital height, bandwidth, and carrier frequency impact the Doppler shift which causes packet losses. To be consistent with [21], we evaluate the performance of the proposed Doppler shift pre-compensation scheme concerning these three parameters. We have satellite telemetry data corresponding to TIANQI-7, which operates on downlink carrier frequency $f_c = 400.45$ MHz and $h = 518$ km. We extrapolate our data to evaluate the validity of the proposed idea across different orbital heights, uplink carrier frequencies, and channel bandwidths. In Fig. 6, Fig. 7 and Fig. 8, the color code specified in the legend allows us to distinguish whether the transmitted uplink packet was successfully received by satellite or failed due to excessive Doppler shift.

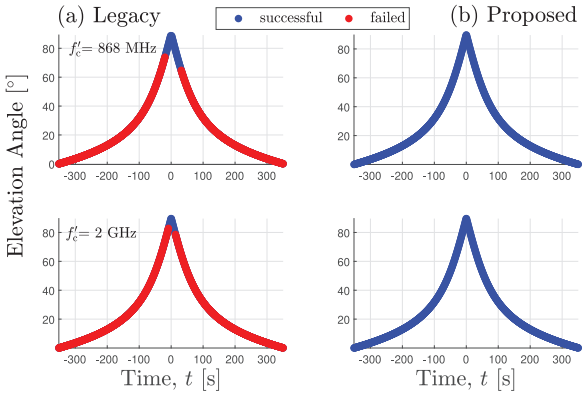

FIGURE 7. Comparison of LoRa DtS packet losses due to Doppler shift at $h = 518$ km and $B_{\text{uplink}} = 31.25$ kHz for $f_c' = 868$ MHz and $f_c' = 2$ GHz, without (legacy) and with the proposed pre-compensation scheme.

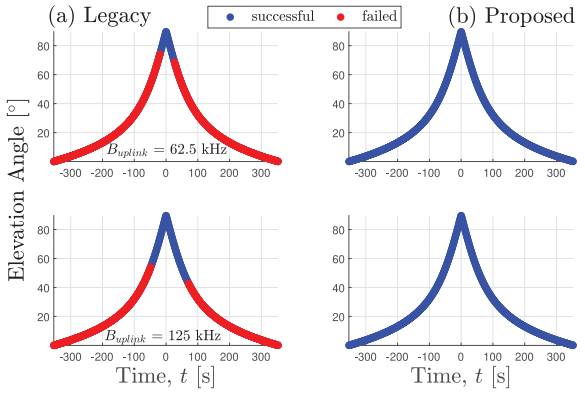

FIGURE 8. Comparison of LoRa DtS packet losses due to Doppler shift at $f_c' = 2$ GHz and $h = 518$ km for $B_{\text{uplink}} = 62.5, 125$ kHz, without (legacy) and with the proposed pre-compensation scheme. The upper part of the figure shows results for an LEO satellite operating with $B_{\text{uplink}} = 62.5$ kHz and the lower part of the figure reveals results for $B_{\text{uplink}} = 125$ kHz.

1) ORBITAL HEIGHT

In the upper plot of Fig. 6 (a), which refers to $h = 518$ km, $f_c' = 401.45$ MHz and $B_{\text{uplink}} = 31.25$ kHz, it is observed that the Doppler shift the leads to packet loss for $\theta \leq 53°$ and $\theta \leq 23°$ when $t \leq 0$ and $t > 0$, respectively. These losses occur because Doppler shift exceeds the tolerance threshold $f_{\text{static}} = \pm 0.25 \times B_{\text{uplink}} = \pm 7.8$ kHz, for these values of θ. The asymmetrical behavior of these results is consistent with the lower plot of Fig. 4, where the Doppler shift is higher in the time window $t \leq 0$ compared to time $t > 0$. The primary reason for this asymmetrical behavior is the offset between the crystal oscillator of the satellite and the end device used to estimate FEI. However, with the implementation of the proposed pre-compensation scheme, no packet losses due to Doppler shift were observed in the uplink as shown in the upper plot of Fig. 6 (b).

Very low Earth orbit (VLEO) satellites are designed to orbit at an altitude between 200 km and 350 km. VLEO satellites provide the benefit of a lower path loss but entail a stronger Doppler effect and greater synchronization challenges. The lower plot of Fig. 6 (a) evaluates the performance of the proposed scheme for a VLEO satellite at $h = 200$ km. One can see that legacy LoRa DtS is affected by packet loss for $\theta \leq 55°$ and $\theta \leq 30°$ when $t \leq 0$ and $t > 0$, respectively. In the lower plot of Fig. 6 (b), it is evident that our framework effectively pre-compensates the Doppler shift and delivers all packets successfully.

2) CARRIER FREQUENCY

In Europe and North America, LoRa operates at 868 MHz and 915 MHz, respectively. The newer models of LoRaWAN end devices also support the S-band for satellite IoT connectivity.

To assess the validity of the proposed approach across different uplink carrier frequencies, we extrapolate our data (see Section V-B) to various frequencies. Specifically, at $f_c' = 868$ MHz and $f_c' = 2$ GHz, the Doppler shift exceeds 20 kHz and 47 kHz, respectively, for a satellite orbiting at 518 km. Due to low tolerance threshold $f_{\text{static}} = \pm 7.8$ kHz, LoRa DtS experience significant packet losses. Fig. 7 illustrates how the proposed Doppler shift pre-compensation solution succeeds in avoiding packet losses due to Doppler shift in 868 MHz and 2 GHz bands.

3) BANDWIDTH

In Fig. 8, we evaluate the effectiveness of the proposed framework across $f_c' = 2$ GHz, $h = 518$ km and for different uplink bandwidths such as $B_{\text{uplink}} = 62.5$ kHz and $B_{\text{uplink}} = 125$ kHz. The upper plot of Fig. 8 (a) presents the results for $B_{\text{uplink}} = 62.5$ kHz. The results show that the Doppler shift causes packet loss for $\theta \leq 74°$ when $t \leq 0$ and for $\theta \leq 69°$ when $t > 0$. The lower plot of Fig. 8 (a) shows results for $B_{\text{uplink}} = 125$ kHz, where Doppler shift causes packet loss for $\theta \leq 54°$ when $t \leq 0$ and for $\theta \leq 43°$ when $t > 0$. In Fig. 8 (b), the results demonstrate that the proposed framework successfully pre-compensates for the Doppler shift, ensuring the delivery of all packets.

C. MINIMUM REQUIRED DOPPLER BEACON BANDWIDTH

The satellite's orbital height h, minimum elevation angle θ_{min}, and carrier frequency f_c are the primary factors influencing the maximum Doppler shift $\max(f_d)$ in channel, and consequently selection of a suitable B_{downlink}, as discussed in Section II-B. We use (5) and (7) to examine $\max(f_d)$ and needed B_{downlink}, respectively. The left-hand side of Fig. 9 depicts the maximum Doppler shift, $\max(f_d)$, in the channel for different orbital heights including VLEO, LEO, and medium Earth orbit (MEO).

The analysis considers minimum elevation angles of $\theta_{\text{min}} = 0°$ and $\theta_{\text{min}} = 40°$, along with carrier frequencies of $f_c = 433$ MHz, 868 MHz, 2 GHz. Given these parameters, Fig. 9 illustrates the minimum required downlink bandwidth, B_{downlink}, for a satellite's Doppler Beacon. As the orbital altitude increases, the required B_{downlink} decreases due to the reduced Doppler effect at higher altitudes. The minimum

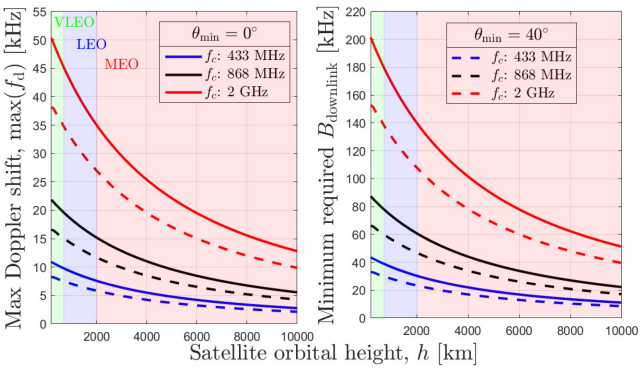

FIGURE 9. The left-hand side of the figure shows maximum Doppler shift (max(f_d)) in the channel for different orbital heights including VLEO, LEO, and MEO with minimum elevation angle $\theta_{\min} = 0°$ and $\theta_{\min} = 40°$, and carrier frequencies $f_c = 433$ MHz, 868 MHz, 2 GHz. The right-hand side of the figure demonstrates the minimum required Doppler beacon bandwidth (B_{downlink}) for these parameters.

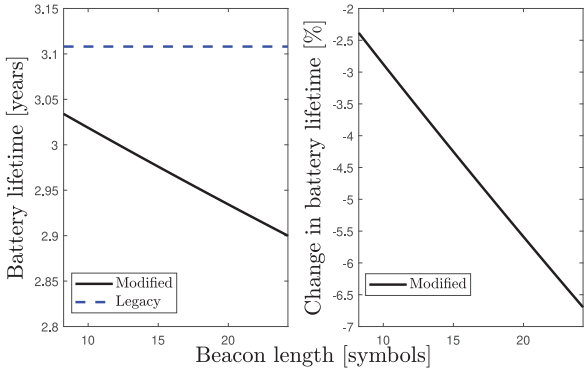

FIGURE 10. Comparison of legacy and modified LoRaWAN end device operation battery lifetime.

elevation angle, $\theta_{\min}$, defines the visibility window, the maximum coverage area, and the maximum Doppler shift experienced by the satellite. Notably, a higher $\theta_{\min}$ results in a smaller coverage area and a lower Doppler shift compared to a lower $\theta_{\min}$. Therefore, for $\theta_{\min} = 40°$, a narrower B_{downlink} is required for the Doppler Beacon.

Additionally, the carrier frequency f_c, which is directly proportional to the Doppler shift, plays a crucial role in determining B_{downlink}. For example, at $f_c = 433$ MHz, the required B_{downlink} is 43.6 kHz for $\theta_{\min} = 0°$ and decreases to 33 kHz for $\theta_{\min} = 40°$. At $f_c = 868$ MHz, these values increase to 87.4 kHz and 66.34 kHz, respectively. In the S-band at 2 GHz, the required B_{downlink} further increases to 201.5 kHz for $\theta_{\min} = 0°$ and 152.8 kHz for $\theta_{\min} = 40°$, respectively. We expect these results to help practitioners and researchers choose suitable settings.

D. ENERGY CONSUMPTION

The benefits of the proposed Doppler shift pre-compensation schemes incur additional energy consumption due to RX0 before every uplink transmission. In this section, we assess the impact on energy consumption by (i) comparing the battery lifetime in years of an IoT end device for legacy and proposed LoRaWAN operations, and (ii) calculating the percentage change in battery lifetime for the modified operation compared to the legacy LoRaWAN operation. We consider an end device with a battery capacity of 230 mAh, transmitting a 10-byte packet every $T_{\text{notification}} = 900$ seconds. We use the LoRa energy consumption model from the Semtech datasheet (refer to *Section II-B. Class A Energy Profile* [50]). We apply the number of symbols in a Doppler Beacon from $N\text{sym} = 8.25$ to 25. We set RX0 duration twice as long than the Doppler Beacon's time-on-air t_b. As in [50], we apply the minimum RX1 and RX2 wake-up time of 5 symbols. As illustrated in Fig. 10, the energy consumption related to RX0 is on the order of a few percent compared to the energy consumption of legacy LoRaWAN operation. At this marginal cost, the proposed Doppler shift pre-compensation solution effectively combats the strong Doppler shift in the LEO scenario.

VII. DISCUSSION AND FUTURE WORK

The proposed modification to LoRaWAN Class A operation can be implemented through software updates to open the window RX0 for Doppler pre-compensation. Notably, the proposed framework does not require any hardware modifications to the end device, which ensures compatibility with existing end devices. Our results confirm the effectiveness of the proposed Doppler shift pre-compensation solution. However, there remains a need to address several open challenges and research questions to optimize the key parameters and generalize this solution. Below, we highlight some selected interesting directions that, from our standpoint, seem particularly relevant.

A. OPTIMAL BEACON DESIGN AND PARAMETERS

This work presents a baseline Doppler Beacon design. Further research is required to determine whether shorter or longer preambles or differently designed preambles would be more effective for Doppler shift pre-compensation. It is worth mentioning that opening RX0 for an interval t_{rx0} introduces an additional energy consumption. A beacon comprising just a few chirps can help reduce the potential energy consumption due to RX0. Additionally, we believe it essential to investigate the optimal SF for Doppler Beacon transmission by the LEO satellite, which requires further studies. The LoRa SFs directly impacts the chirp duration and associated energy consumption. For example, SF7, which provides the shortest chirp duration (lowest t_b), may help to minimize energy consumption. On the downside, SF7 also poses challenges due to its critical link budget requirements [19], [20]. On the satellite side, it is important to investigate the timing and scheduling of Doppler Beacons to ensure their continuous transmission.

B. GENERALIZATION OF THE PROPOSED SOLUTION

All LoRaWAN end devices start in Class A as a baseline operation mode. Moreover, most existing literature on

LoRaWAN DtS assumes the use of Class A end devices [11], [19], [20], [41], [44], [45]. This motivated our decision to consider Class A end devices as the baseline scenario for our proposed approach. We conjecture that our solution can also be extended to legacy Class B and Class C end devices; however, further research is required to assess the applicability of the proposed scheme to these device classes.

Particularly, a Class B end device periodically opens its receive window to enable downlink communication and receive time-synchronized network beacons. In principle, the device can also apply LoRa's built-in FEI mechanism to the beacons for estimating the Doppler shift. It is important to note, in this regard, that Class B beacons are transmitted with a fixed region-specific configuration, such as fixed coding rate and payload length, and the preamble is longer than the default one. For instance, in the European region, the Class B beacon uses SF9, bandwidth of 125 kHz, resulting in an airtime of 160 ms and approximately 39.06 symbols [53], and is broadcast at 869.525 MHz [53]. This implies that the satellite would need to switch from one beacon format to another while orbiting the Earth.

Moreover, in Class B networks, synchronization beacons are transmitted by network gateways every 128 seconds. This presents several challenges for the proposed solution, as follows:

- To detect the non-continuous Doppler beacon, the device must keep its receiver active for at least one beacon period, which requires RX0 duration t_{rx0} to be longer than 128 seconds, thereby significantly increasing energy consumption.
- A satellite may be visible to the end device for less than 128 seconds, which could result in the Class B device missing a beacon during the satellite pass.
- LoRaWAN Class A end devices use an ALOHA-type protocol for accessing the uplink channel, allowing them to operate without requiring time synchronization between the network server and the end device. Unlike Class A operation, a Class B end device opens extra receive window at the scheduled time and receives a time synchronized Beacon from the gateway. This step synchronizes end device and the network server. The mobility of LEO satellites and the time-varying propagation delay could pose challenges for the time synchronization for LoRaWAN Class B end devices.
- In terrestrial LoRaWAN networks, the network server uses signal quality indicators from the most recent uplink transmission by the Class B end device to select the appropriate gateway for beacon transmission [53]. However, this approach will require that each satellite carries a network server onboard, which presents several drawbacks, as discussed in [19], [20]. Due to the mobility of satellites, achieving real-time coordination among all network servers within the constellation to access the signal quality from the latest uplink from a specific end device may be challenging.
- If a Class B end device cannot receive beacons, it will expand the reception windows of the beacon and ping slot (downlink slots), leading to increased energy consumption. Despite the extended slots, if the device does not receive a beacon during these periods, it will revert to legacy Class A operational mode, which does not listen for beacons..
- In addition to these challenges, in the case of non-continuous Doppler Beacons the risk of uplink transmission collisions increases when multiple end devices successfully receive the same beacon and estimate the Doppler shift. This occurs because multiple end devices may receive the same Doppler Beacon simultaneously thereby attempting simultaneous uplink transmissions after processing the same beacon.

Finally, Class C devices enhance the capabilities of Class A end devices by keeping receive windows open at all times, except when transmitting an uplink packet. Class C end devices can also perform LoRa's built-in FEI mechanism if the satellite either periodically or continuously transmits the beacons. However, this constant receive mode results in significantly higher energy consumption, making Class C end devices impractical for long-term battery-powered operation and thus failing to meet a crucial requirement for satellite IoT applications [11].

C. EXTENSION TO LR-FHSS

LoRaWAN protocol offers two modulation schemes, namely, conventional chirp-based LoRa and Long Range-Frequency Hopping Spread Spectrum (LR-FHSS). In this paper, motivated by massive deployment [11], [14], [18], [19], [20], [21], [41], [46], [47] as well as the high availability of real-world LoRa satellite data [15], we propose and validate a Doppler shift pre-compensation solution specifically for the conventional LoRa modulation scheme. LR-FHSS is a new technology introduced in the LoRaWAN protocol, specifically designed to meet the requirements of satellite IoT applications [54], [55]. Differently from LoRa, which uses CSS modulation, LR-FHSS employs Gaussian Minimum Shift Keying (GMSK) modulation with frequency hopping. Within LoRaWAN, LR-FHSS supports only uplink communications from end devices to satellites, while the downlink uses conventional LoRa modulation. To the best of our knowledge, no existing research assesses the impact of the Doppler effect on LR-FHSS DtS connectivity. Given that the downlink of LR-FHSS end devices supports typical LoRa modulation, our designed LoRa Doppler Beacon and proposed Doppler shift pre-compensation solution could potentially be adopted for LR-FHSS DtS connectivity. We consider it worth investigating how the proposed solution could benefit LR-FHSS DtS communication.

D. COUNTERMEASURES AGAINST JAMMING AND SPOOFING

Spoofing and jamming may pose serious challenges to the effectiveness of the proposed solution by disrupting the

accuracy of Doppler shift pre-compensation [56]. A jammer is likely to be a terrestrial device. The coverage of terrestrial LoRa networks is generally limited to a few kilometers. Consequently, the impact of a jammer would be limited to a small area. One notable feature of LoRa modulation is the capture effect, which allows the end device to recover the Doppler beacon despite interference from a jamming signal. This occurs when the received power of the Doppler beacon exceeds the jamming signal by at least 6 dB [20]. In future work, we consider it important to explore the effects of these threats, taking into account the jammer distance, power levels, and bandwidth, as well as identifying suitable countermeasures to ensure the solution remains robust and reliable. To address potential interference from jamming, a promising approach is to increase the number of RX0 estimations. By using both the Doppler shift and Doppler rate, it may more effectively differentiate the true Doppler Beacon signal from any jamming-induced distortions. This approach could enhance the robustness of Doppler shift estimation and mitigate the impact of jamming on the pre-compensation process, thereby reducing packet loss and improving performance.

VIII. CONCLUSION

This paper has proposed a method that enables end devices in a LoRa DtS link to estimate and pre-compensate for the Doppler shift before initiating an uplink transmission to the satellite. The several presented results confirm the feasibility and robustness of the proposed pre-compensation scheme. As a next step, we plan to develop a proof-of-concept to test the practicality of this idea under different channel conditions and communication settings in the laboratory environment. Specifically, we plan to conduct laboratory experiments using an SDR-based Doppler emulator to further validate our findings in controlled conditions. We consider it worth investigating how the proposed scheme behaves for different radio access technologies, frequency bands, end device models, satellites, and their orbits. To further support the presented approach, in future works, we intend to design a LoRa satellite Doppler Beacon to use limited frequency resources efficiently and reduce the RX0 energy consumption. We will consider extending this work for predicting the distance between end device and satellite. This will allow us to enable Adaptive Data Rate, i.e., SF allocation mechanism which will further enhance the LoRa DtS communications performance. We will also extend our future work to theoretically evaluate the bit error rate and throughput gain, providing deeper insights into the communication performance of the proposed framework. Finally, future work should explore advanced modulation schemes, including OTFS and AFDM, to leverage Doppler diversity gain for improved DtS communication performance.

REFERENCES

[1] A. Maleki, H. H. Nguyen, E. Bedeer, and R. Barton, "A tutorial on chirp spread spectrum modulation for LoRaWAN: Basics and key advances," *IEEE Open J. Commun. Soc.*, vol. 5, pp. 4578–4612, 2024.

[2] B. A. Homssi, K. Dakic, S. Maselli, H. Wolf, S. Kandeepan, and A. Al-Hourani, "IoT network design using open-source LoRa coverage emulator," *IEEE Access*, vol. 9, pp. 53636–53646, 2021.

[3] O. Kodheli et al., "Satellite communications in the new space era: A survey and future challenges," *IEEE Commun. Surveys Tuts.*, vol. 23, no. 1, pp. 70–109, 1st Quart., 2021.

[4] O. Georgiou and U. Raza, "Low power wide area network analysis: Can LoRa scale?" *IEEE Wireless Commun. Lett.*, vol. 6, no. 2, pp. 162–165, Apr. 2017.

[5] W. Wu and W. Wang, "Preamble structure and timing advance method for satellite IoT," *IEEE Wireless Commun. Lett.*, vol. 13, no. 4, pp. 1088–1092, Apr. 2024.

[6] R. Marini et al., "Low-power wide-area networks: Comparison of LoRaWAN and NB-IoT performance," *IEEE Internet Things J.*, vol. 9, no. 21, pp. 21051–21063, Nov. 2022.

[7] M. Chiani and A. Elzanaty, "On the LoRa modulation for IoT: Waveform properties and spectral analysis," *IEEE Internet Things J.*, vol. 6, no. 5, pp. 8463–8470, Oct. 2019.

[8] G. Pasolini, "On the LoRa chirp spread spectrum modulation: Signal properties and their impact on transmitter and receiver architectures," *IEEE Trans. Wireless Commun.*, vol. 21, no. 1, pp. 357–369, Jan. 2022.

[9] M. Centenaro et al., "A survey on technologies, standards and open challenges in satellite IoT," *IEEE Commun. Surveys Tuts.*, vol. 23, no. 3, pp. 1693–1720, 3rd Quart., 2021.

[10] J. A. Fraire, S. Céspedes, and N. Accettura, "Direct-to-satellite IoT—A survey of the state of the art and future research perspectives: Backhauling the IoT through LEO satellites," in *Proc. 18th Int. Conf. Ad-Hoc Netw. Wireless*, Luxembourg, Luxembourg, 2019, pp. 241–258, doi: 10.1007/978-3-030-31831-4_1.

[11] M. A. Ullah, K. Mikhaylov, and H. Alves, "An overview of direct-to-satellite IoT: Opportunities and open challenges," in *Proc. IEEE 9th World Forum Internet Things (WF-IoT)*, 2023, pp. 1–8.

[12] M. A. Ullah, F. Clazzer, A. Munari, K. Mikhaylov, and H. Alves, *An Overview of Medium Access Control Protocols in Machine-Type Communication Satellite Internet-of-Things Networks*. Hoboken, NJ, USA: Wiley, 2024, ch. 6, pp. 119–146.

[13] A. M. Zadorozhny et al., "First flight-testing of LoRa modulation in satellite radio communications in low-earth orbit," *IEEE Access*, vol. 10, pp. 100006–100023, 2022.

[14] V. Y. Prokopyev et al., "NORBY CubeSat nanosatellite: Design challenges and the first flight data," *J. Phys. Conf.*, vol. 1867, no. 1, Apr. 2021, Art. no. 12038.

[15] TinyGS. "TinyGS, the open source global satellite network." Accessed: Sep. 16, 2024. [Online]. Available: https://tinygs.com/satellites

[16] C. C. Chan, A. Al-Hourani, J. Choi, K. M. Gomez, and S. Kandeepan, "Performance modeling framework for IoT-over-satellite using shared radio spectrum," *Remote Sens.*, vol. 12, no. 10, p. 1666, 2020.

[17] T. N. González et al., "Analysis of channel models for LoRa-based direct-to-satellite IoT networks served by LEO nanosatellites," in *Proc. IEEE Int. Conf. Commun. Workshops (ICC Workshops)*, 2021, pp. 1–6.

[18] F. A. Tondo et al., "Multiple channel LoRa-to-LEO scheduling for direct-to-satellite IoT," *IEEE Access*, vol. 12, pp. 30627–30637, 2024.

[19] M. A. Ullah, K. Mikhaylov, and H. Alves, "Massive machine-type communication and satellite integration for remote areas," *IEEE Wireless Commun.*, vol. 28, no. 4, pp. 74–80, Aug. 2021.

[20] M. Asad Ullah et al., "Enabling mMTC in remote areas: LoRaWAN and LEO satellite integration for offshore wind farms monitoring," *IEEE Trans. Ind. Informat.*, vol. 18, no. 6, pp. 3744–3753, Jun. 2022.

[21] M. A. Ullah et al., "Understanding the limits of LoRa direct-to-satellite: The doppler perspectives," *IEEE Open J. Commun. Soc.*, vol. 5, pp. 51–63, 2024.

[22] A. A. Doroshkin et al., "Experimental study of LoRa modulation immunity to doppler effect in CubeSat radio communications," *IEEE Access*, vol. 7, pp. 75721–75731, 2019.

[23] A. Doroshkin et al., "Laboratory testing of LoRa modulation for CubeSat radio communications," in *Proc. MATEC Web Conf.*, vol. 158, 2018, p. 1008.

[24] G. Colavolpe, T. Foggi, M. Ricciulli, Y. Zanettini, and J.-P. Mediano-Alameda, "Reception of LoRa signals from LEO satellites," *IEEE Trans. Aerosp. Electron. Syst.*, vol. 55, no. 6, pp. 3587–3602, Dec. 2019.

[25] M. A. Ullah. "Extending the LoRa direct-to-satellite limits: The doppler shift pre-compensation scheme." Accessed: Mar. 17, 2025. [Online]. Available: https://github.com/MuhammadAsadUllah1/LoRa-Doppler-Shift-Pre-Compensation.git
[26] A. Al-Hourani and B. A. Homssi, "Doppler shift distribution in satellite constellations," *IEEE Commun. Lett.*, vol. 28, no. 9, pp. 2131–2135, Sep. 2024.
[27] B. A. Homssi and A. Al-Hourani, "Optimal beamwidth and altitude for maximal uplink coverage in satellite networks," *IEEE Wireless Commun. Lett.*, vol. 11, no. 4, pp. 771–775, Apr. 2022.
[28] Semtech. "SX1276/77/78/79—137 MHz to 1020 MHz low power long range transceiver." Accessed: Sep. 16, 2024. [Online]. Available: https://www.semtech.com/products/wireless-rf/lora-connect/sx1276
[29] Semtech. "SX1268 long range, low power, sub-GHz RF transceiver." Accessed: Sep. 16, 2024. [Online]. Available: https://www.semtech.com/products/wireless-rf/lora-connect/sx1268
[30] Semtech. "Application note: LoRa® modulation crystal oscillator guidance." Accessed: Sep. 16, 2024. [Online]. Available: https://www.semtech.com/products/wireless-rf/lora-connect/sx1276
[31] Semtech. "AN1200.80—LoRa® modem doppler immunity AppNote." Accessed: Sep. 16, 2024. [Online]. Available: https://www.semtech.com/products/wireless-rf/lora-edge/lr1120
[32] Semtech. "AN1200.64 LR-FHSS system performance." Accessed: Sep. 16, 2024. [Online]. Available: https://www.semtech.com/products/wireless-rf/lora-edge/lr1120
[33] R. M. Colombo, A. Mahmood, E. Sisinni, P. Ferrari, and M. Gidlund, "Low-cost SDR-based tool for evaluating LoRa satellite communications," in *Proc. IEEE Int. Symp. Meas. Netw. (M N)*, 2022, pp. 1–6.
[34] Y. Ge, L. Meng, D. G. González, M. Wen, Y. L. Guan, and P. Fan, "Linear precoding design for OTFS systems in time/frequency selective fading channels," *IEEE Wireless Commun. Lett.*, vol. 14, no. 3, pp. 816–820, Mar. 2025.
[35] Y. Tao, M. Wen, Y. Ge, J. Li, E. Basar, and N. Al-Dhahir, "Affine frequency division multiplexing with index modulation: Full diversity condition, performance analysis, and low-complexity detection," 2025, *arXiv.2411.09938*.
[36] J. Kang et al., "Regression based pilot design for doppler effect estimation and compensation in LEO satellite communication with LoRa," in *Proc. 27th Asia–Pac. Conf. Commun. (APCC)*, 2022, pp. 631–632.
[37] X. Lin, S. Rommer, S. Euler, E. A. Yavuz, and R. S. Karlsson, "5G from space: An overview of 3GPP non-terrestrial networks," *IEEE Commun. Stand. Mag*, vol. 5, no. 4, pp. 147–153, Dec. 2021.
[38] X. Lin, Z. Lin, S. E. Löwenmark, J. Rune, R. Karlsson, and Ericsson, "Doppler shift estimation in 5G new radio non-terrestrial networks," in *Proc. IEEE Global Commun. Conf. (GLOBECOM)*, 2021, pp. 1–6.
[39] L. Schulthess, T. Salzmann, C. Vogt, and M. Magno, "A LoRa-based energy-efficient sensing system for urban data collection," in *Proc. 9th Int. Workshop Adv. Sensors Interfaces (IWASI)*, 2023, pp. 69–74.
[40] Semtech. "LoRa edge™ tracker reference design user guide." [Online]. Available: https://lora-developers.semtech.com/uploads/documents/files/LoRa_Edge
[41] M. A. Ullah, A. Yastrebova, K. Mikhaylov, M. Höyhtyä, and H. Alves, "Situational awareness for autonomous ships in the arctic: MMTC direct-to-satellite connectivity," *IEEE Commun. Mag.*, vol. 60, no. 6, pp. 32–38, Jun. 2022.
[42] J. Wigard et al., "Ubiquitous 6G service through non-terrestrial networks," *IEEE Wireless Commun.*, vol. 30, no. 6, pp. 12–18, Dec. 2023.
[43] T. Bouguera, J.-F. Diouris, J.-J. Chaillout, R. Jaouadi, and G. Andrieux, "Energy consumption model for sensor nodes based on LoRa and LoRaWAN," *Sensors*, vol. 18, no. 7, p. 2104, 2018. [Online]. Available: https://www.mdpi.com/1424-8220/18/7/2104
[44] K. Lin, M. A. Ullah, H. Alves, K. Mikhaylov, and T. Hao, "Subterranean mMTC in remote areas: Underground-to-satellite connectivity approach," *IEEE Commun. Mag.*, vol. 61, no. 5, pp. 136–142, May 2023.
[45] S. Herrería-Alonso, M. Rodríguez-Pérez, R. F. Rodríguez-Rubio, and F. Pérez-Fontán "Improving uplink scalability of LoRa-based direct-to-satellite IoT networks," *IEEE Internet Things J.*, vol. 11, no. 7, pp. 12526–12535, Apr. 2024.
[46] J. A. Fraire, P. Madoery, M. A. Mesbah, O. Iova, and F. Valois, "Simulating LoRa-based direct-to-satellite IoT networks with FLoRaSaT," in *Proc. IEEE 23rd Int. Symp. World Wireless Mobile Multimedia Netw. (WoWMoM)*, 2022, pp. 464–470.
[47] G. Álvarez et al., "Uplink transmission policies for LoRa-based direct-to-satellite IoT," *IEEE Access*, vol. 10, pp. 72687–72701, 2022.
[48] Semtech. "An in-depth look at LoRaWAN® class a devices." Accessed: Aug. 2, 2024. [Online]. Available: https://lora-developers.semtech.com/uploads/documents/files/LoRaWAN_Class_A_Devices_In_Depth_Downloadable.pdf
[49] P. V. Walvekar, "Virtualizing LoRa baseband functionalities to the edge," Ph.D. dissertation, KTH Royal Inst. Technol., Stockholm, Sweden, 2019.
[50] Semtech. "LoRaWAN® device classes." Accessed: Jan. 7, 2025. [Online]. Available: https://www.semtech.com/uploads/technology/LoRa/lorawan-device-classes.pdf
[51] M. A. Ullah, K. Mikhaylov, and H. Alves. "Experiment-based models for air time and current consumption of LoRaWAN LR-FHSS." 2024. [Online]. Available: https://arxiv.org/abs/2408.09954
[52] Federal Communications Commission. "BLUEWALKER 3 NON-GEOSTATIONARY SATELLITE updated technical annex." Accessed: Sep. 16, 2024. [Online]. Available: https://apps.fcc.gov/els/GetAtt.html?id=281537&x=.
[53] Semtech. "An in-depth look at LoRaWAN® class B devices." Accessed: Aug. 2, 2024. [Online]. Available: https://lora-developers.semtech.com/uploads/documents/files/LoRaWAN_Class_B_Devices_In_Depth_Downloadable.pdf
[54] E. Testi and E. Paolini, "Packet collision probability of direct-to-satellite IoT systems," *IEEE Internet Things J.*, vol. 12, no. 2, pp. 1843–1855, Jan. 2025.
[55] M. Asad Ullah, K. Mikhaylov, and H. Alves, "Analysis and simulation of LoRaWAN LR-FHSS for direct-to-satellite scenario," *IEEE Wireless Commun. Lett.*, vol. 11, no. 3, pp. 548–552, Mar. 2022.
[56] N. Hou, X. Xia, and Y. Zheng, "Jamming of LoRa PHY and countermeasure," in *Proc. IEEE INFOCOM Conf. Comput. Commun.*, 2021, pp. 1–10.

MUHAMMAD ASAD ULLAH (Member, IEEE) received the master's and Ph.D. (with Distinction) degrees from the University of Oulu, Finland, in 2020 and 2024, respectively. He is a Senior Scientist with the VTT Technical Research Center of Finland Ltd., Espoo, Finland. From 2018 to 2023, he was with the 6G Flagship, Centre for Wireless Communications, University of Oulu. In 2022, he was a Visiting Researcher with the University of Bologna, Italy, and a Ph.D. student with Nokia, Finland. In 2022, he was a finalist in the Millennium Young Scientist Contest, organized by Technology Academy Finland as part of the Millennium Innovation Forum. His technical expertise includes measurements, analytical, and simulation modeling of wireless communications systems, with a particular focus on nonterrestrial networks and aeronautical telecommunication networks.

RICHARD DEMO SOUZA (Senior Member, IEEE) received the D.Sc. degree in electrical engineering from the Federal University of Santa Catarina (UFSC), Brazil, in 2003. From 2004 to 2016, he was with the Federal University of Technology, Brazil. Since 2017, he has been with UFSC, where he is currently a Professor. His research interests include wireless communications and signal processing. He was a co-recipient of the 2014 IEEE/IFIP Wireless Days Conference Best Paper Award and the Supervisor of the awarded Best Ph.D. Thesis in Electrical Engineering, Brazil, in 2014, and a co-recipient of the 2016 Research Award from the Cuban Academy of Sciences. He has served as an Editor or an Associate Editor for the SBrT *Journal of Communications and Information Systems*, the IEEE COMMUNICATIONS LETTERS, IEEE TRANSACTIONS ON VEHICULAR TECHNOLOGY, IEEE TRANSACTIONS ON COMMUNICATIONS, and the IEEE INTERNET OF THINGS JOURNAL.

GIANNI PASOLINI (Member, IEEE) is an Associate Professor with the Department of Electrical, Electronic and Information Engineering, University of Bologna, where he has been teaching various courses in the field of telecommunications since 2003. He is one of the Founding Member with the "National Laboratory of Wireless Communications (Wilab), National Inter-University Consortium for Telecommunications (CNIT), Italy. Throughout his career, he has actively participated in several European initiatives focused on wireless communications, including COST actions and Networks of Excellence. His research interests encompass wireless communication systems, Internet of Things, digital signal processing, and THz communications. He serves as an Associate Editor for the IEEE OPEN JOURNAL OF THE COMMUNICATIONS SOCIETY. He served as a member of the organizing committee for several IEEE conferences.

JEAN MICHEL DE SOUZA SANT'ANAA (Member, IEEE) received the D.Sc. (tech.) degree in communications engineering from the University of Oulu, Oulu, Finland, in 2023. Since 2019, he has been with the 6G Flagship, Centre for Wireless Communications, University of Oulu, where he is a Postdoctoral Researcher. His interests are in machine-type communications, nonterrestrial networks, and network simulation.

MARKO HÖYHTYÄ (Senior Member, IEEE) is an Associate Professor for Technology Foresight and Adaptation with the Finnish National Defence University, Finland. He was a Research Professor of Satellite Communications with the VTT Technical Research Centre of Finland Ltd. He has over 20 years' experience in connectivity technology research and development both for terrestrial and satellite networks. In addition to his Finnish National Defence University position, he is a docent with the University of Oulu. He has roughly 100 scientific publications in journals and conferences and he has authored a book *Satellite Communications and Networks*. He is regularly an invited speaker and a panellist in international conferences, providing visionary insights to the broad fields of SatComs and critical communications.

KONSTANTIN MIKHAYLOV (Senior Member, IEEE) is an Associate Professor for Convergent IoT Communications for Vertical Systems with the Centre for Wireless Communications, University of Oulu. The major focus of his research is on radio access and beyond-access technologies for massive and dependable IoT and the matters related to the design and performance of IoT devices and systems. He has authored or coauthored about 100 research contributions on wireless connectivity for IoT, system design, and applications. He is the WG3 Network Architectures and Protocols Co-Chair for COST action CA20120 "INTERACT", the Co-Chair of SAT-IoT in 2023, WEAR-IoT from 2019 to 2024 and EN-IoT from 2024 to 2025 Workshops, and the Track Co-Chair of EuCNC 2022 and 2025.

HIRLEY ALVES (Member, IEEE) is currently an Associate Professor and the Head of the Machine-Type Wireless Communications Group, 6G Flagship, Centre for Wireless Communications, University of Oulu. He actively works on massive connectivity and ultra-reliable low latency communications for future wireless networks, 5GB and 6G, full-duplex communications, and physical-layer security. In addition, he leads the URLLC activities for the 6G Flagship Program. He has received several awards and has been the organizer, the chair, the TPC, and a tutorial lecturer for several renowned international conferences. He is the General Chair of the ISWCS'2019 and the General Co-Chair of the First 6G Summit, Levi 2019, and ISWCS 2021.

ENRICO PAOLINI (Senior Member, IEEE) received the Dr.Ing. degree (summa cum laude) in telecommunications engineering and the Ph.D. degree in electrical engineering from the University of Bologna, Italy, in 2003 and 2007, respectively. While working toward the Ph.D. degree, he was a Visiting Research Scholar with the Department of Electrical Engineering, University of Hawai'i at Manoa, Honolulu, HI, USA. He was a Visiting Scientist with the Institute of Communications and Navigation, German Aerospace Center in 2012 and 2014, under DLR-DAAD Fellowships. He is currently an Associate Professor with the Department of Electrical, Electronic, and Information Engineering, University of Bologna. His research interests include digital communication systems, error correcting codes, massive multiple access protocols, and detection and tracking in radar systems. He served as the Co-Chair for the ICC 2014, ICC 2015, and ICC 2016 Workshop on Massive Uncoordinated Access Protocols (MASSAP), the VTC 2019-Fall Workshop on Small Data Networks, the 2018 IEEE European School of Information Theory, and the 2020 IEEE Information Theory Workshop. He served as the TPC CoChair for the IEEE GLOBECOM 2022–CT and the IEEE GLOBECOM 2019–CT. He is a Past Chair of the ITSoc Italy Section Chapter and the Chair of the IEEE ComSoc Radio Communications Committee. He was an Editor of IEEE COMMUNICATIONS LETTERS from 2012 to 2015 and the IEEE TRANSACTIONS ON COMMUNICATIONS (in coding and information theory) from 2015 to 2020.

AKRAM AL-HOURANI (Senior Member, IEEE) received the Ph.D. degree from RMIT University in 2016. He is a Professor and the Discipline Leader of the Department of Electrical and Electronic Engineering, School of Engineering, RMIT University, Melbourne, Australia. He is also the Deputy Director of the Centre for Opto-Electronic Materials and Sensors and the Telecommunication Program Manager (Masters). He previously worked as a Research and a Development Program Manager in the satellite and telecommunication industry, where he directed industry projects valued at over $120 million. With his expertise, he is currently engaged in multiple research and industry projects related to satellite communications, synthetic aperture radar, and AI in wireless communications. As the Lead Investigator, he played a crucial role in delivering the largest open Internet-of-Things network in Victoria in collaboration with five local governments, the Northern Melbourne Smart Cities Network. He contributed to over 120 journal articles and conference proceedings and is currently ranked in the top 2% of scientists worldwide according to Stanford University's latest rankings, in both the Career-Long and Single Year Impact categories. His research interests include satellite communications, radar systems, neuromorphic computing, signal processing/machine learning, and stochastic geometry. This project won two prestigious industry awards: The Technology Awards for Excellence from the Municipal Association of Victoria and the Smart Cities Award from the IoT Alliance Australia. He is also a recipient of the Alexander von Humboldt Fellowship for Experienced Researchers 2024 in Spaceborne Synthetic Aperture Radar with the German Aerospace Center (DLR) and the Academic of the Year Space Award in 2024 Australia. He is currently an Associate Editor in multiple high-impact journals, including IEEE TRANSACTIONS OF AEROSPACE AND ELECTRONICS.